EU Horizon program: Horizon-CL4-2021-TWIN Transition

Reducing environmental footprint, improving circularity in extractive and processing value chains (IA)

Grant Agreement No 101058310

WP 7 Handling & sorting of fine fraction

D7.1. Report on bulk powder characteristics and direct sorting methods

ReSoURCE

Project Reference No	101058310
Deliverable	D7.1. Report on bulk powder characteristics and direct sorting methods
Workpackage	WP7
Type	R
Dissemination Level	PU
Date	November 2023
Status	Final
Editor(s)	Kristin Søiland, Chandana Ratnayake, Simone Neuhold, Florian Feucht, Karl Friedrich
Contributor(s)	SINTEF, RHIM, MUL
Reviewers	All partners
Document description	This deliverable reports powder properties and identified direct sorting methods for leftover breakout material < 5 mm of spent refractory.

Document revision history

Version	Date	Modification introduced	
		Modification reason	Author
V0.1		1st version	SINTEF
V1.0	28.11.2023	Final	SINTEF

Executive Summary

This deliverable presents the powder properties and chemical composition of leftover spent refractory below 5 mm of grain size. The leftovers are from two sources, cement rotary kiln (CRK) and steel casting ladle (SCL). Experiments with different dry separation processes has been conducted, with the purpose of removing dust particles and impurities as a pretreatment before recycling as new refractory products. Experimental tests with cross-flow air classification, single- and multi-chamber fluidization classifiers have been carried out. Fluidization has been proven as a suitable classification method for separating dust and lighter particles from the leftover material pre-sieved at 1 mm.

Table of Contents

1. Materials and Methods

Separation of powders in dry form is a fundamental process utilized across various industries and applications. This method involves the extraction and division of solid particulate matter based on their distinctive properties, such as size, density, shape, or electrostatic charge, without the involvement of any liquid or solvent. One of the most common techniques for dry powder separation is sieving, which uses a mesh or screen to sift particles based on their size. Another prevalent method is air classification, where air flow is used to separate particles based on their aerodynamic properties. Dry powder separation is crucial in fields like pharmaceuticals, food processing, mining, and agriculture, where achieving the desired particle size distribution or isolating specific components is essential for product quality, safety, and efficiency. This process not only enhances product quality but also reduces waste and resource consumption.

The reader is referred to a comprehensive overview [1] that discusses air classification devices, encompassing their operational principles, characteristics, and key parameters such as cut size, cleanness, and recovery. In practical applications, a range of gravitational and centrifugal classifiers is utilized, including those featuring vertical and horizontal air streams, cascade classifiers, fluidized bed separators, inertial, vortex, rotor classifiers, and more. The selection of classifier types and designs is influenced by technological needs (such as throughput and cleanness) and the specific properties of the materials undergoing classification [2].

In this chapter some principals of direct sorting techniques are described. In Table 1 below some commonly used terms in this deliverable report are described.

Table 1 Glossary with common terms used in this deliverable report.

Term	Description
Refractory leftover	After breaking out a refractory lining that has reached its end of life in service, the fraction <80 mm is called the leftover. Larger particles and bricks are sorted manually and recycled in different ways.
Angle of Repose	Is the maximum angle at which a powder or particulate material will remain stable without flowing or sliding.
Powder classifier	A device used to separate and classify powdered materials based on their particle size, shape, or other specific properties.
Fine/coarse fraction	After separation with a classifier device, the powder material is separated in one or several fine and coarse fractions.
Particle size distribution	The range of particle sizes present in a sample of material, indicating the relative proportions of different particle sizes within that sample.
Cut-size	The cut size represents the particle size at which 50% of the powder material has a smaller particle size, and 50% is larger.
Fluidization	A process where solid particles are suspended and behave like a fluid when subjected to a

	flowing gas or liquid. In this report fluidization is used as a separating technique.
Steel casting ladle	Is a ladle used to transport the liquid steel from the furnace to the casting bed.
Cement rotary kiln	A slowly rotating furnace used in the process of making cement. Reaches temperatures up to 1450°C.
SCL	In this context the SCL refers to the spent refractory removed from a steel casting ladle.
CRK	In this context the CRK refers to the spent refractory removed from a cement rotary kiln.

1.1 Tromp Curve

The term 'Tromp curve' typically refers to a graphical representation of the performance of a particle separation device, such as a classifier, in terms of particle size distribution [3]. It is commonly used in the context of analysing the efficiency of air classifiers or other similar devices. The Tromp curve plots the cumulative distribution of the feed material against the cumulative distribution of the product and the coarse material. This curve helps in understanding the efficiency of the separation process. The curve can provide valuable information about the overall efficiency of the separation process, including the sharpness of separation and the amount of fine, mid and coarse particles present. Understanding the Tromp curve is crucial in optimizing the performance of particle separation processes and in identifying potential areas for improvement. It helps in evaluating the effectiveness of different operating conditions and in assessing the quality of the final product obtained from the separation process.

1.2 Sharpness of Separation (SoS)

The sharpness of separation (SoS) in a Tromp curve is a measure of the effectiveness of a particle separation process [4]. It quantifies how well a classifier or separator can differentiate between particles of different sizes. The SoS in a Tromp curve is typically calculated using the cut size (d50) and the width of the distribution. The cut size represents the particle size at which 50% of the material is smaller and 50% is larger. The width of the distribution is often determined by the spread of the curve around the cut size. A commonly used measure for SoS is the partition curve's slope around the cut size. A steeper slope indicates a higher sharpness of separation, suggesting that the classifier can more effectively differentiate between particles of different sizes. Mathematically, the SoS can be estimated by examining the rate of change of the Tromp curve around the cut size, often by calculating the derivative or slope of the Tromp curve at the specified point. A higher slope indicates a sharper separation, while a flatter slope suggests a less effective separation process.

The Imperfection Factor (IF) is typically calculated using the Tromp curve, which represents the partition curve for a particle separation process. The IF is often derived from the area under the Tromp curve.

1.3 Imperfection Factor (IF)

The general approach to calculating the IF involves comparing the actual separation achieved by the equipment to the ideal separation that would occur in a perfect system. The detail of simplified methods to calculate the IF is find somewhere else [5]. The IF helps in quantifying the inefficiencies or

imperfections in the separation process. A value of 0 indicates perfect separation, while a value closer to 1 signifies a less effective or imperfect separation process.

1.4 Geldart's powder groups

Before doing separation experiments based on a material's fluidization properties, critical parameters such as Geldart's powder group and fluidization properties such as minimum fluidization velocity must be explored. Geldart's classification of powders was first reported in 1973 and describes the behaviour of powders in fluidized beds depending on the particle size and density [6]. The Geldart diagram in Figure 1 gives a first expectation how a specific powder will behave when fluidized, but practical tests are usually also needed to show the full picture. Using a fluidization column more fluidization parameters can be investigated. There the different powder groups will look something like the examples in Figure 2.

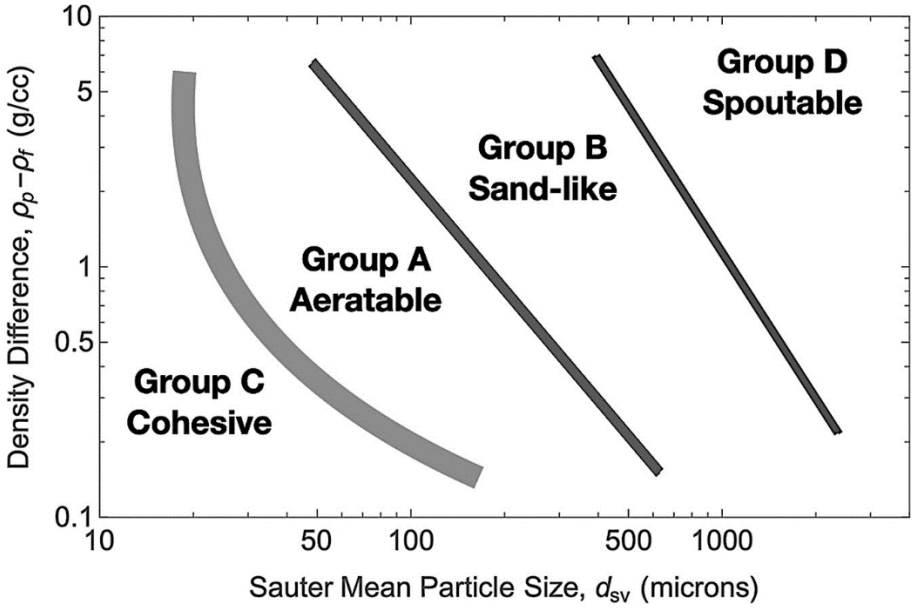

Figure 1 Geldart powder groups [7].

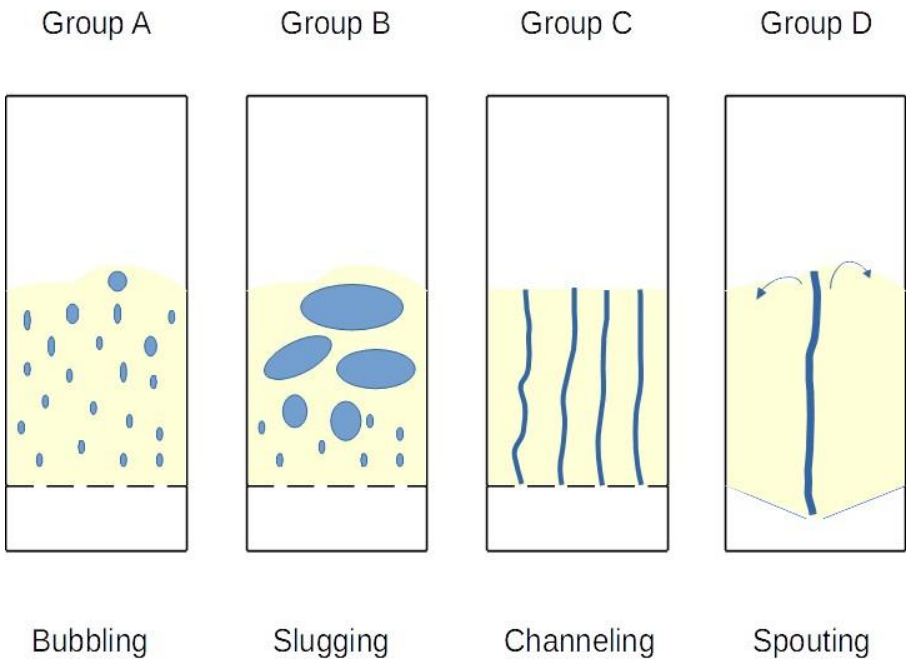

Figure 2 Behaviour of different powder groups under fluidization [8].

In a fluidization column, the pressure drop over the powder bed is measured. The gas velocity is slowly increased and the powder bed height measured. Plotting the gas velocity and the pressure drop is one way of finding the minimum fluidization velocity, as shown in Figure 3. At this gas velocity, the powder particles is starting to behave like a fluid or become suspended. At this velocity, the drag force exerted by the fluid on the particles is enough to balance the force of gravity acting on them, causing the particles to become buoyant and preventing them from settling or packing together. This is a critical point in fluidization processes and is used to design and operate fluidized bed reactors.

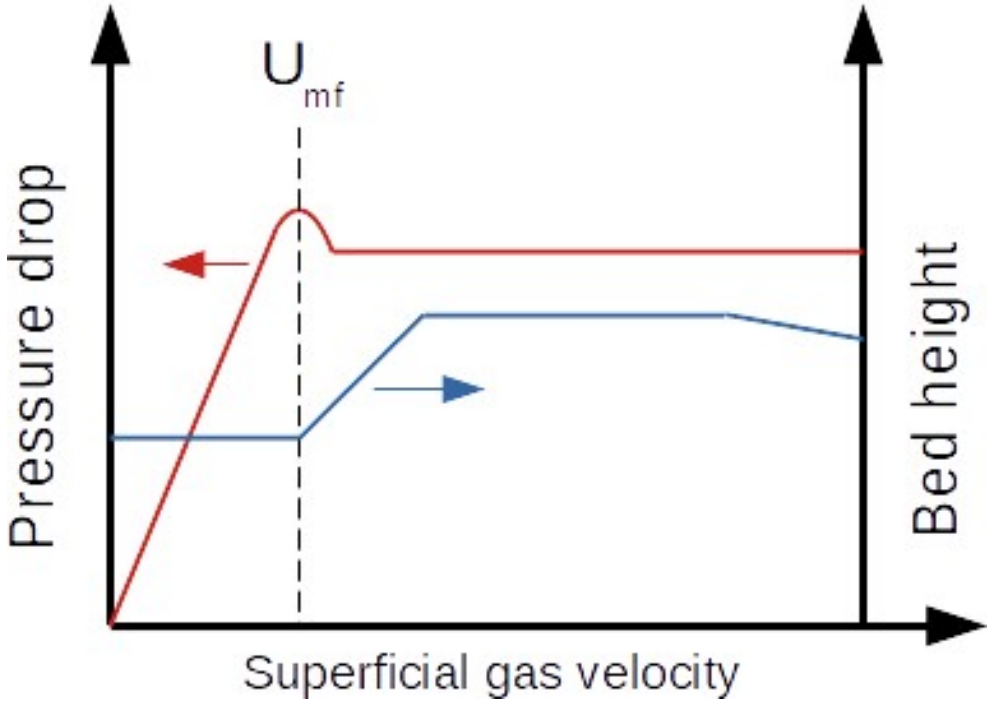

Figure 3 Minimum fluidization velocity [8].

2. State of the Art Analysis

A market study of available classification equipment has been performed to see if there is suitable equipment available on the market for similar material to the refractory leftover. The findings are presented in Table 2. Similar materials are handled in e.g., the mining or sand/gravel industry.

A general finding is that the classifiers are often used in combination with a mill to ensure homogenous size distributions and some equipment needs to be fitted to each specific use case, thus technical data is not available. For some products the mill is an integrated part in the classifier device. Avoiding the milling step is reducing the total energy consumption when recycling the leftover material, and therefore beneficial in the ReSoURCE project, unless milling is proven to increase the yield. The leftover material received for testing has a wide particle size distribution from 0 to 5 mm, which is wider than some of the classification equipment available handles without milling or other preprocess steps.

Table 2 Market study of available classification equipment suitable for leftover refractory <5 mm.

Description of equipment	**Supplier**	**Evaluation**	**Link**
Classifier mill	Bauermeister	1-20 kg feed capacity with cyclone separation. 97% under 3 µm output. Small lab scale device.	https://www.bauermeister.de/en/Machines/Air-Classifiers/laboratory-classifier-mill/
Static spiral flow classifier	Bauermeister	Throughput 500-3000 kg. No operational data available, needs to be customized for each use case.	https://www.bauermeister.de/en/Machines/Air-Classifiers/static-spiral/
Air classifier CL	Bauermeister	Exists in 7 different sizes, cut point range 8-160 µm. For applications that needs ultra-fine particle sizes.	https://www.bauermeister.de/en/Machines/Air-Classifiers/air-classifier/
Centrifugal sifting and size control	Gericke	Can be placed directly in the transportation line, mostly used in food-industry. Suitable for diluted phases when using pneumatic conveying. Suitable for dedusting. Separation of particles according to size from 40 µm to 5 mm. 2-3 kg/hour up to 120 tonnes/hr. Rotary mesh inside the unit, sieves the product. Several sizes available, determines the capacity. Only examples of soft powders like flour, PVC, cosmetics available online.	https://www.gerickegroup.com/fileadmin/user_upload/Downloads/Brochures/UK/661_4_UK_Gericke_Brochure_Sifter.pdf
C-line traditional vibrating sieves	Virto	Single and multiple decks with sieves, portable and fixed version available. Many sizes, mesh sizes. Batch separation.	https://www.virtogroup.com/productline/c-l/

Construction and demolition waste recycling	Metso	Huge installations for mining, quarries, contractors. Both mobile and stationary equipment. For transport, screening and crushing of material. Crushing down to more uniform grain size for easier handling.	https://www.metso.com/aggregates/solutions/construction-and-demolition-waste-recycling/
Fisher Air Separator	Fisher Industries	Portable, several models between 60 - 150 tonnes per hour capacity for 10 mm product. Used for sand, silica, gravel etc. Not suitable for dedusting. Transport using conveying belt, open system	https://www.fisherind.com/air-separator
V7 Dry sand making system	Kemco	Crusher with interacted air screen. Has increased the production of 0.6 - 0.15 mm particles.	https://www.kemco.co.jp/eng/pdf/kemco_v7.pdf
Electrostatic separator	Stokkermill	Usually used for metals and plastic separation. Electrostatic properties of refractory must be investigated to find out if this is suitable.	https://www.stokkermill.com/recycling-machines/electrostatic-separator-for-separation
Vertical Pilot Plant Centrifuge Chemical	Heinkel	Separation of solids from liquid. Liquid process not considered at this stage.	https://www.heinkel.com/product/vertical-pilot-plant-centrifuge-chemical/
Air classifier CL	Alpha Powder Equipment	Need to be contacted for details. Vertical and horizontal rotor. Single and multi-rotor available. Also available in combination with milling.	https://www.alpapowder.com/machines/classifier/
Dust removal and collection	Alpha Powder Equipment	Mainly filter bag type. No standard equipment needs to be specified for each costumer.	https://www.alpapowder.com/removal-and-collection/
Classifier	Powder Systems	High precision classifier separates in three different particle sizes. Classification size 3-200 µm, 1-3000 kg/h	https://www.powder.co.jp/EN/products/01/
Mikro ACM Air Classifying Mill	Hosokawa Micron Powder system	Grinds the material down to <20 µm, available from laboratory scale up to process production.	https://www.hmicronpowder.com/mikro-acm-air-classifying-mill/
Alpine Ventoplex Air Classifier	Hosokawa Micron Powder system	The classifier wheel is changeable, thus allows a wide range in particle size separation. Classifies based on centrifugal and flow forces. Suitable for mineral industry. Fitness range from 24-200 µm.	https://hmicronpowder.com/alpine-ventoplex-air-classifier/

3. Description of Material

3.1 Motivation and suitable sorting techniques

Refractory bricks are produced in a wide variety of compositions, tailor-made for the costumers needs. In the steel casting ladle, the magnesium oxide is mixed with graphite to achieve the properties needed in service. When breaking out the spent lining, it is needed to remove as much as possible of the carbon before recycling. The most energy efficient way of removing carbon particles from the refractory leftover is by using dry direct sorting methods. There is a significant difference in density between graphite and MgO, which indicates that a direct sorting could be possible. Observed in the initial chemical analysis of the SCL leftover, is an enrichment of carbon content in the smallest size fraction. This observation could indicate that a removal of the finest particles of the SCL leftover material could reduce the total content of carbon and simultaneously reduce the dust content.

When handling the leftover material, there is a huge amount of dust generated because of the high content of small particles. Dust generation is a major risk to the people handling the material and to the surroundings environment. Operators have a potential risk of inhaling hazardous particles that can cause severe damage to the respiratory system. The surrounding ecosystem can suffer from pollution of dust particles, which over time can threaten vulnerable ecosystems. Observed dust in local communities has also been in focus among the local population and authorities in areas close to industrial sites. Wide support among the locals is always of importance to be allowed to operate the industry in that area. Recycling of the finest fraction of the refractory material will therefore have to consider the dust generation when handling the material.

The experimental work in this deliverable has been carried out to minimize or eliminate the risk of dust generation and to ensure an energy efficient separation of carbon of the SCL before further recycling. Other possible variations in composition after sorting based on the powder properties like size and density will also be investigated.

Given the material properties and characteristics, air supported classification techniques have been considered as most suitable for the material. The separation methods separate the material based on size and density differences in the different particles and can handle ultra fine particles up to the coarser region of 1-5 mm particles. The classification methods need to be experimental tested and optimized for the desired outcome.

3.2 Origin and Sampling Procedure

Refractory products are used in high-temperature industrial processes (e.g., steel, cement, or glass production), protecting process units such as furnaces or hot metal ladles against chemical, mechanical and thermal stresses. The refractory lining is designed for a specific application with defined process conditions. After end-of-life, the lining is dismantled, and the material removed, whereby neither the mixing of different product types and qualities nor the abrasion of the bricks and the generation of fine fractions due to handling and transportation can be effectively avoided.

Sorting the material before recycling it in new refractory products is therefore essential. However, manual sorting is still state-of-the-art for break-out material, leading to restrictions based on the grain size. Material smaller than 70 to 80 mm cannot be sorted manually due to economic reasons and is currently mainly landfilled or downcycled in products such as metallurgical additives. In the course of the project ReSoURCE new possible application areas for the fine fraction will be exploited and a direct

sorting method for the fraction 0-5 mm will be developed. As currently planned for the automated sorting, different material streams will be available for sampling and further used in subsequent tasks. After characterization, the feedstock material will be pre-processed and classified into fine grain sizes <5 mm and coarse grain sizes >5 mm. The coarse fraction will pass demonstrator A, the fine fraction will be treated by direct sorting methods and demonstrator B.

For this purpose, the fine fraction 0-5 mm of so-called leftovers of two aggregates, a steel casting ladle break-out material (SCL) and a cement rotary kiln break-out material (CRK), were provided by RHIM for further investigations. These leftover samples correspond to the representative sampling campaigns described in D1.1 and D1.2. After manual sorting of the sampled piles (CRK 150 t and SCL 25 t), material that is too fine for manual sorting is dropped from the conveyor belt into big bags. Per aggregate, one of these big bags was further processed at RHIM. The samples were screened into the fractions > 30 mm; 10-30 mm; 5-10 mm and 0-5 mm. Samples were taken at certain time intervals during the sieving process to obtain representative samples per grain fraction. To investigate possible direct sorting approaches, the 0-5 mm fraction was further screened into the sub-fractions 0-0.25 mm; 0.25-0.5 mm; 0.5-1.0 mm; 1.0-3.0 mm and 3.0-5.0 mm. A total of 200 kg per aggregate were provided by RHIM.

3.3 Analysis of the Leftover Material

The sub-fractions of the samples described in section 3.2 were analysed chemically and mineralogically at RHIM. For main oxides X-ray fluorescence analysis (XRF) was carried out using a Bruker Austria GmbH, S8 Tiger, a CS-744 LECO system was used for determining the carbon and sulphur content; the mineralogical investigations were performed on a Bruker D8 Advance for X-ray diffraction (XRD) including Rietveld refinement. In addition, other possible infiltrations besides carbon and sulphur (i.e., K_2O, Na_2O and Cl) were analysed for CRK using optical emission spectroscopy by inductively coupled plasma (ICP-OES) according to ISO 26845 and titration, respectively.

For the SCL break-out material, an enrichment of carbon in the form of graphite in the finest fraction (0-0.25 mm) is recognizable, for CRK break-out material, an increase in concentration of infiltrating elements, especially K_2O, Cl and carbon is noticeable, leading to the formation of e.g., sylvite (KCl) and calcite ($CaCO_3$).

3.4 Scanning electron microscopy (SEM) analysis

During the material characterization conducted in WP 3, the relationship between chemical-mineralogical composition and grain size was examined within the 0 - 5 mm leftover fraction of CRK and SCL using a scanning electron microscope (SEM). This analysis furthermore enabled the identification of contaminations and their distribution within the material.

Description of the Method

To prepare the samples for SEM analysis, the material was embedded in epoxy resin, sanded, and polished to ensure a smooth surface for analysis. The resulting SEM images, including backscattered electron images and element mappings, were analysed using the open-source image processing software Fiji, a distribution of ImageJ. After setting the corrected scale, each image was cropped to remove any scale bars or written text. The images were then transformed into 8-bit to enable threshold adjustments. Mineral phases were identified by overlaying different element maps and determining areas where elements co-occur. The final images were then analysed by measuring the Feret diameter and area of each grain of a mineral phase.

The Feret diameter was used to assign each mineral grain into grain size classes. The total area was calculated for each grain size class and each mineral type. Finally, the share of each mineral phase within these ranges was determined. Grains consisting of different agglomerated or associated mineral phases were assigned to the mineral phase that occurs most frequently within the grain. Grains located at the edge of the image section, which are only partially visible, are still considered in this evaluation.

Using this data, distribution of mineral composition and mineral distribution over the grain size can be presented. The results are used as an indicator on the possibility to enrich mineral phases or increase yield using classification by grain size. Since grain size classes were chosen arbitrarily and technological limitations are not considered at this point, the results do not contain an evaluation of actual processability of the material. The results obtained should be interpreted as a trend, which can be supported by further analysis of grain size fractions produced in WP 7 and further SEM evaluations in WP 3.

Deliverable 1.2 describes the presence of alkali salts and -sulphates as impurities within CRK samples, thereby classifying chemical constituents such as K, Na, Cl, and S as undesirable by-products. In contrast, the SCL material exhibited lower levels of impurity infiltration but higher levels of adhesion of impurities. As a result, slags and their chemical composition, characterized by increased concentrations of Si, Ca, and Al, are considered as impurities. The evaluation of Cl from the element maps was not feasible due to the presence of Cl as a component of the epoxy resin utilized for embedding the material.

Carbon, which is an essential part of refractory bricks typically utilized in SCL, is also a component of the epoxy resin which complicates a clear identification via SEM analysis. Nonetheless, it was feasible to identify regions through previous light microscopic examination, which are evidently not part of the epoxy resin. These regions also showed elevated C concentrations, which can be seen on the element maps and are therefore assigned to be graphite (Figure 6).

Results CRK

Periclase (MgO) occurs in sizes ranging from 11 - 1800 µm and occupies approximately 42 % of the examined image section. Periclase is present as individual grains, as agglomerated particles of varying sizes, as well as in association with spinel or calcium silicate phases. Spinel ($MgAl_2O_4$) found within the examined section ranges in size from 14 - 856 µm and occupies 4 % of the area. Hercynite ($FeAl_2O_4$) was identified once and has a size of 642 µm. Minerals containing Ca and Si are often found in association with periclase in interparticle areas or pores and less frequently as individual grains. Identified individual Ca + Si mineral phases ranges in size from 5 - 610 µm and occupy 4.2 % of the image section analysed.

The undesired accompanying elements K, Na, and S often occur together and can be found in interparticle areas and pores, or in peripheral areas, as frequently identified in the case of K (Figure 4).

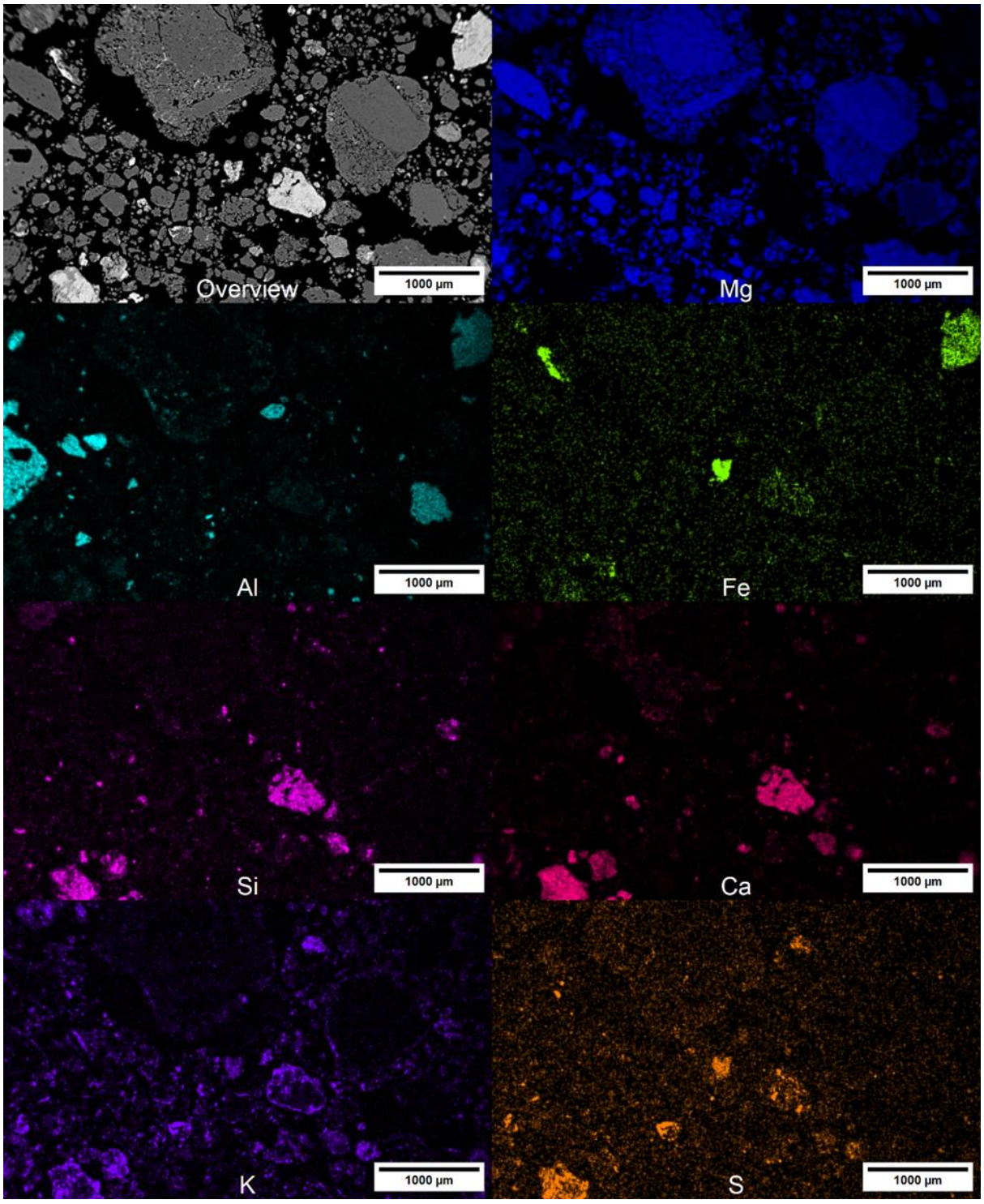

Figure 4 Assembly of element maps of CRK. The high presence of MgO, the co-occurrence of Ca + Si and K + S as well as the increased occurrence of K in peripheral areas can be observed.

The results indicate that minerals containing Ca and Si are more affected by impurities (Figure 5). A grain size range for K, Na or S-containing minerals could not be determined. Since the elements K, Na, and S are frequently found together, the shared surface area is reported being 9.8 %. The remaining screen area (40 %) is occupied by free space.

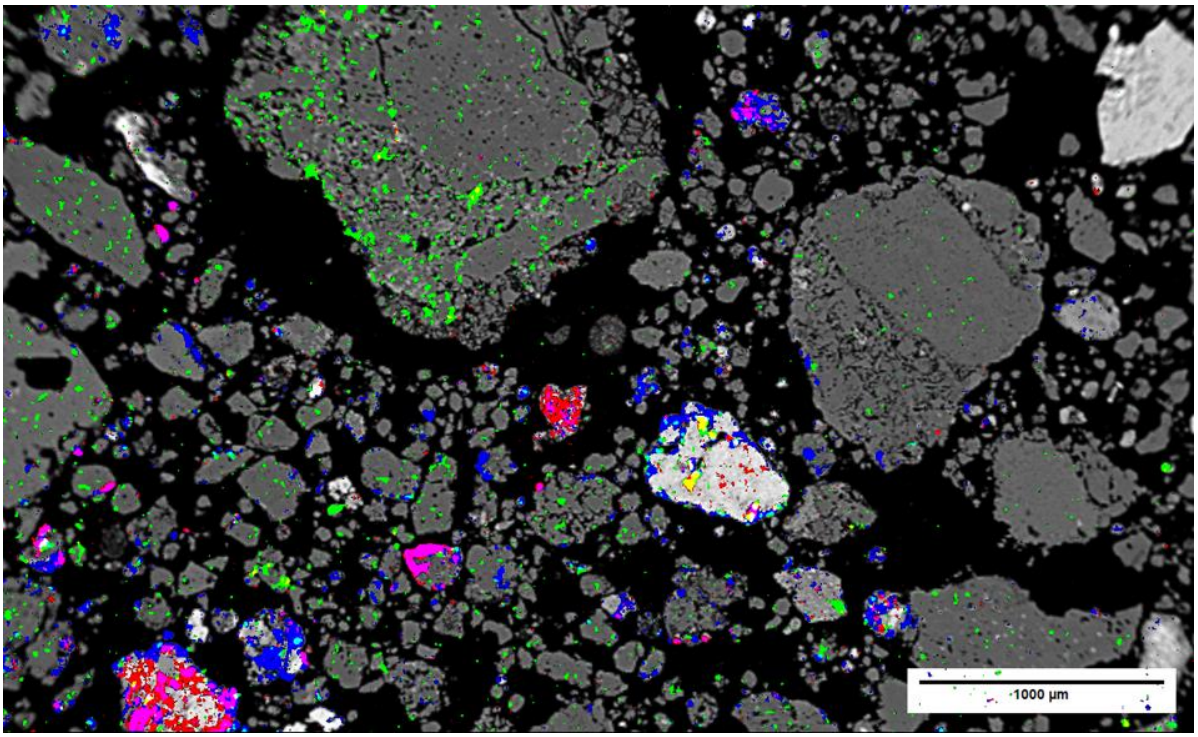

Figure 5 CRK: Element maps of K (blue), Na (green) and S (red) overlaying the backscatter electron image of the analysed section. Magenta indicates areas where K and S are present, while yellow marks areas where Na and S co-occur.

Results SCL

In the analysed image fused periclase grains with a total size up to 4070 µm can be seen with Ca + Si and Ca + Al phases in their interstices. Graphite is expected in areas where C is enriched in comparison to the epoxy (Figure 6). Therefore, four agglomerated MgO grains with Graphite matrix could be identified with a size ranging between 773 – 1451 µm. The respective areas marked in Figure 6 are considered as whole, sortable MgO grains for further evaluation. The analysed image section consists of 48 % pores/free space, 43 % MgO and 3 % C.

The mineral Al_2O_3 could be identified 27 times of which 5 grains are agglomerated with periclase in a graphite matrix or associated with periclase. The respective size ranges from 8 - 488 µm. In total 11 individual SiO_2 grains with a size range from 8 - 234 µm were measured.

The mixed element mineral phases Ca + Si, Ca + Al as well as Al + Si were identified and are displayed in Figure 7. Calcium-silicon phases and Ca + Al can be found in interparticle areas of periclase or associated with periclase and as individual grains with a size ranging from 9 - 147 µm and 38 - 453 µm respectively. In total 16 Ca + Si and 13 Ca + Al individual grains where measured. The mineral phase Al + Si could be identified in the form of two individual grains with a size of 147 µm and 478 µm.

The remaining 6 % of the analysed image section can be subdivided in 1 % Al_2O_3, 0.24 % Al + Si, 0.27 % SiO_2, 0.85 % Ca + Si, 0.40 % Ca + Al and 3.2 % of, to this point of the evaluation, unknown mineral phases.

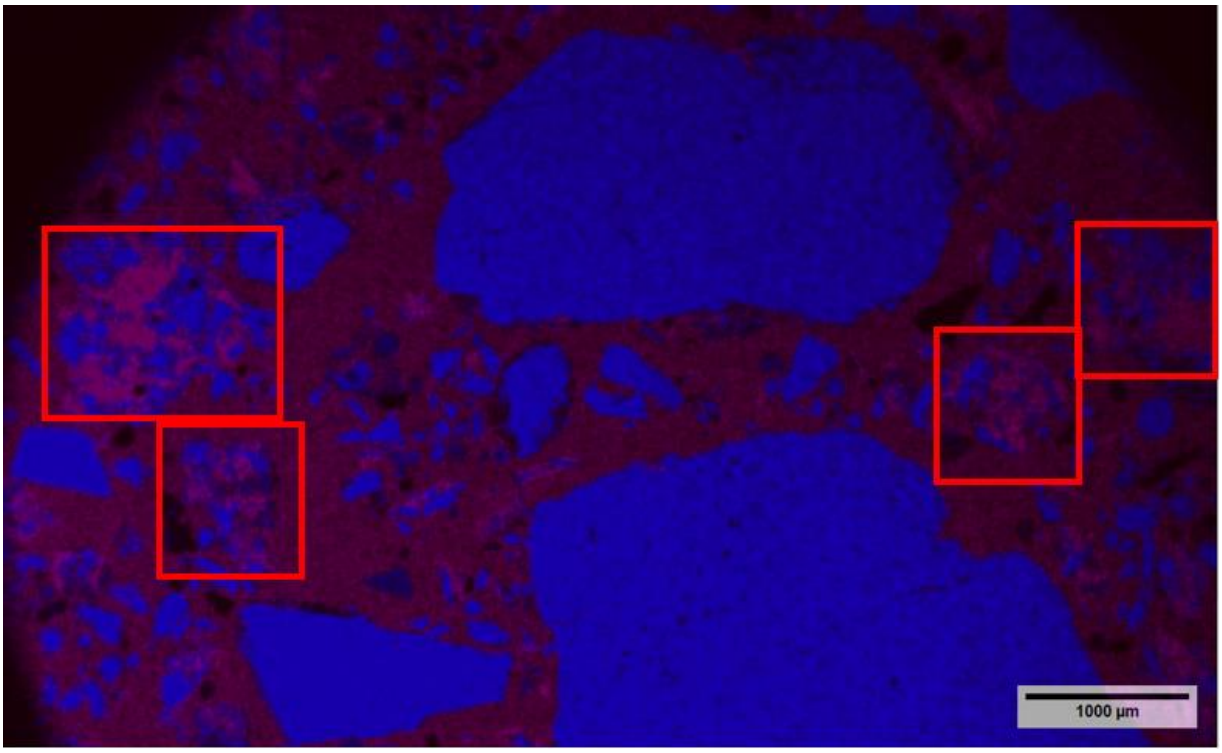

Figure 6 Overlay of two element maps. Mg = blue; C = magenta. Marked areas represent mineral grains of mainly MgO within a graphite matrix.

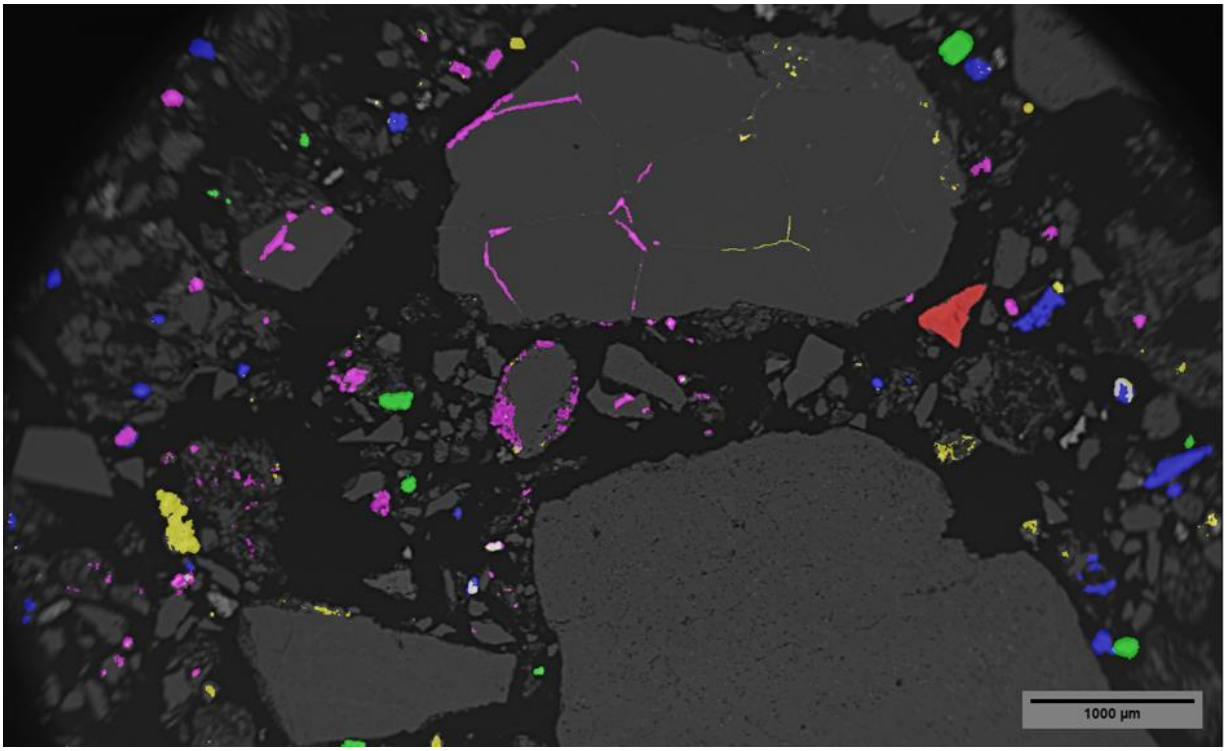

Figure 7 MgO (dark grey) Al_2O_3 (blue), SiO_2 (green), Ca + Si (magenta), Ca + Al (yellow), Al + Si (red). The colour white representing areas where Ca + Al occurs.

3.5 Powder Properties

Density

The particle densities were measured using an auto pycnometer with helium gas. The instrument measures the density of the particles. The results are presented in Table 3. The general trend is an increased particle density with increased size. The trend corresponds well to the chemical analysis where more lighter components like carbon in the SCL and calcite in CRK have a higher concentration in the smaller particle sizes.

Table 3 Particle density of leftover refractory material for different size classes.

Size fraction	CRK [g/cm^3]	SCL [g/cm^3]
0-0.25 mm	2.99	3.20
0.25-0.5 mm	3.03	3.35
0.5-1 mm	3.08	3.62
1-3 mm	3.17	3.59
3-5 mm	3.30	3.64

Angle of repose

The angle of repose is an important parameter in powder handling and bulk material handling because it provides critical information about the flowability and handling characteristics of powders and granular materials. The angle of repose is defined as the steepest angle at which a pile of granular material remains stable without collapsing. Knowledge of the angle of repose helps in the design of handling equipment, such as hoppers, chutes, and conveyors. Equipment can be designed to match the flow characteristics of the material, ensuring efficient and reliable handling.

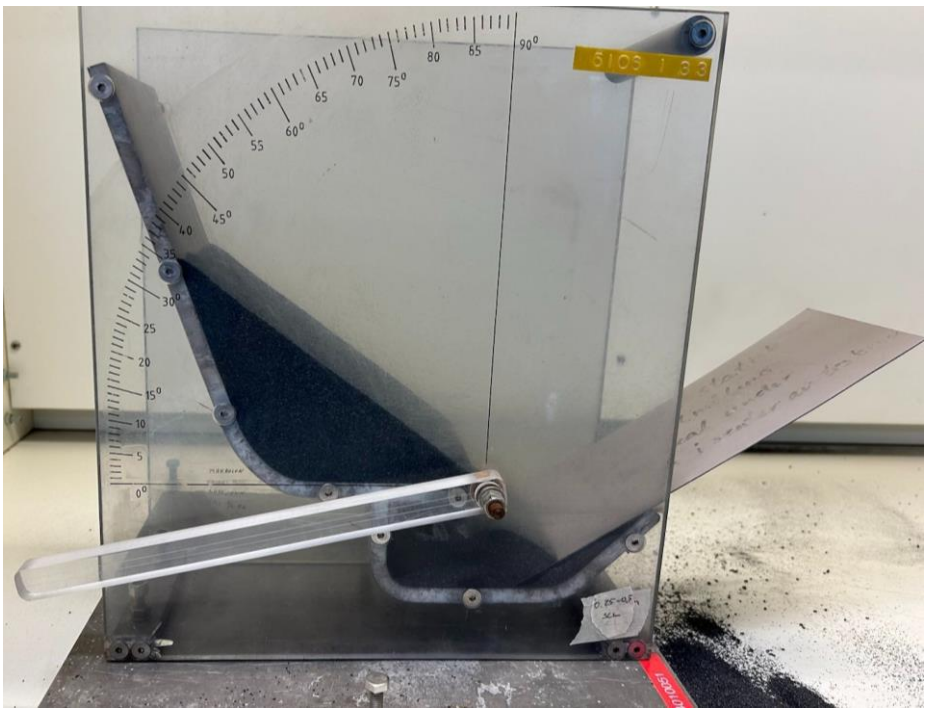

Figure 8 Angle of repose tester.

In ReSoURCE the angle of repose will be an important input to the design of demonstrator B, and for the evaluation of direct sorting techniques. The device used for measuring static and dynamic angle of

repose is shown in Figure 8. The measured angles are given in Table 4. The materials show a free-flowing characteristics in dry state, which means easier handling and storage possibilities. Segregation will depend on PSD of the material, and for the full range of 0-5 mm, the segregation will be significant and considered in the design of demonstrator B.

Table 4 Angle of repose measurements of different size fraction of leftover spent refractory.

	SCL		CRK	
Size fraction	**Dynamic [°]**	**Static [°]**	**Dynamic [°]**	**Static [°]**
0-0.25 mm	37	39	35	37
0.25-0.5 mm	36	36	35	35.5
0.5-1 mm	37	37	37	37
1-3 mm	39	39	40	39
3-5 mm	41	42	41	42
Leftover 0-5 mm	38	39	37	39

Particle size distribution (PSD)

The particle size distribution was measured using a Helos laser diffraction instrument. One sample from each size fraction was measured three times under the same conditions. The PSD plots are attached in Appendix A.

Material	**Size fraction [mm]**	**x10 [µm]**	**x16 [µm]**	**x50 [µm]**	**x84 [µm]**	**x90 [µm]**
CRK	0-0.25	26.7 ± 0.1	40.4 ± 0.3	110.9 ± 1.3	204.3 ± 1.2	233.0 ± 1.7
CRK	0.25-0.5	179.3 ± 6.4	223.0 ± 4.8	346.1 ± 4.8	472.1 ± 5.7	504.1 ± 4.7
CRK	0.5-1	531.3 ± 1.6	582.8 ± 2.7	809.0 ± 8.5	1061.6 ± 25.8	1131.3 ± 23.4
SCL	0-0.25	27.9 ± 0.1	44.9 ± 0.4	123.8 ± 2.3	212.8 ± 1.6	235.4 ± 1.2
SCL	0.25-0.5	266.7 ± 2.3	296.3 ± 4.2	407.3 ± 3.7	550.9 ± 3.7	592.5 ± 2.6
SCL	0.5-1	536.0 ± 1.6	589.8 ± 3.3	816.7 ± 7.5	1091 ± 19.3	1163.7 ± 22.1

Particle Shape

The particle shape of SCL and CRK leftover was investigated using a QICPIC (QP0357) & RODOS instrument. Sphericity is a shape factor describing how close the shape is to a circle. It is a ratio of the perimeter of the equivalent circle (P_{EQPC}) to the real perimeter measured (P_{real}), described in the following equation:

$$S = \frac{P_{EQPC}}{P_{real}} = \frac{2\sqrt{\pi \mathrm{A}}}{P_{real}}$$

The cumulative distribution plot shows the sphericity distribution in the sample, where the calculated volume percentage of particles is below a certain value. For example, $S_{10,3}$ gives the sphericity value where 10% of the sample volume is below this value. In Figure 9 an example of a cumulative distribution of the CRK 0-0.25 mm size class is shown, where the value of $S_{10,3}$, $S_{16,3}$, $S_{50,3}$, $S_{84,3}$ and $S_{90,3}$ is indicated.

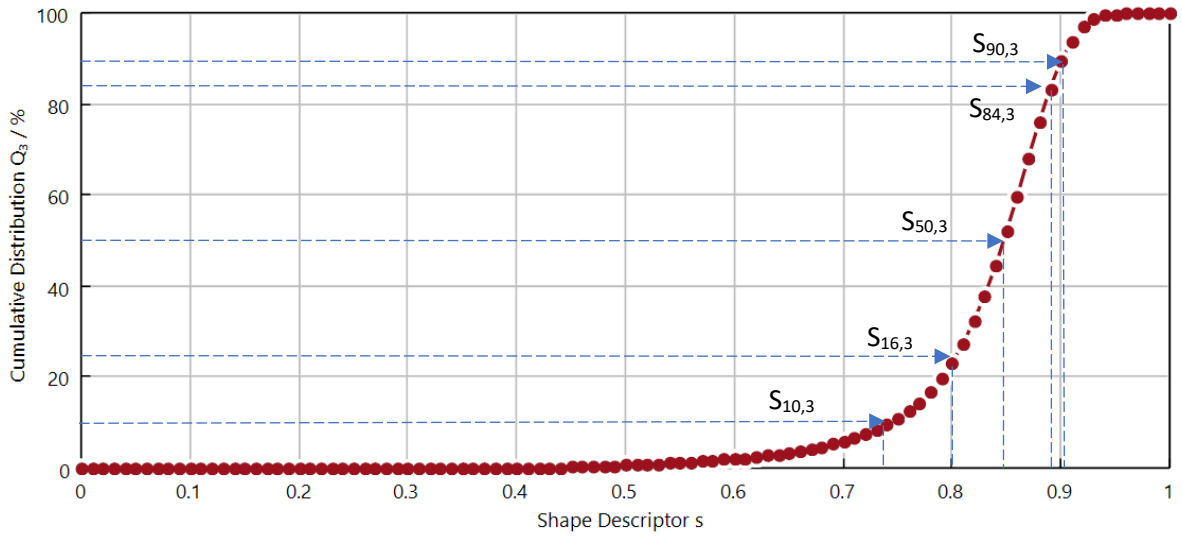

Figure 9 Cumulative sphericity distribution of CRK 0-0.25 mm.

Sphericity distribution plots of the size fraction 0-0.25, 0.25-0.5 and 0.5-1 mm of SCL and CRK are attached in Appendix B. A summary is given in Table 5.

Table 5 Sphericity distribution of particles in CRK and SCL at given size classes.

	CRK			SCL		
Sphericity distribution	0-0.25 mm	0.25-0.5 mm	0.5-1 mm	0-0.25 mm	0.25-0.5 mm	0.5-1 mm
$s_{10,3}$	0.743	0.752	0.746	0.717	0.728	0.721
$s_{16,3}$	0.776	0.769	0.762	0.749	0.747	0.744
$s_{50,3}$	0.847	0.818	0.81	0.824	0.804	0.797
$s_{84,3}$	0.891	0.857	0.846	0.875	0.849	0.845
$s_{90,3}$	0.901	0.866	0.854	0.887	0.86	0.857
$s_{99,3}$	0.935	0.9	0.877	0.927	0.895	0.891

4. Direct Sorting Experiments

Cross-flow air classifier, single- and multi-chamber fluidization have been tested experimentally to reduce the dust content of refractory leftover material, and the removal of carbon from the SCL material has been investigated using fluidization as classification principle. The following chapter describes the experiments and results that have been conducted.

4.1 Cross-flow Air Classification

In process technology, the particle classification stands out as a fundamental operation, pivotal for segregating the provided feed material into two or more distinct fractions, each characterized by varying particle size distributions, density, and other distinct particle properties. The crossflow air classifier, falling under the category of dry-state classification, offers a notable advantage by swiftly generating multiple fractions from a particle collection.

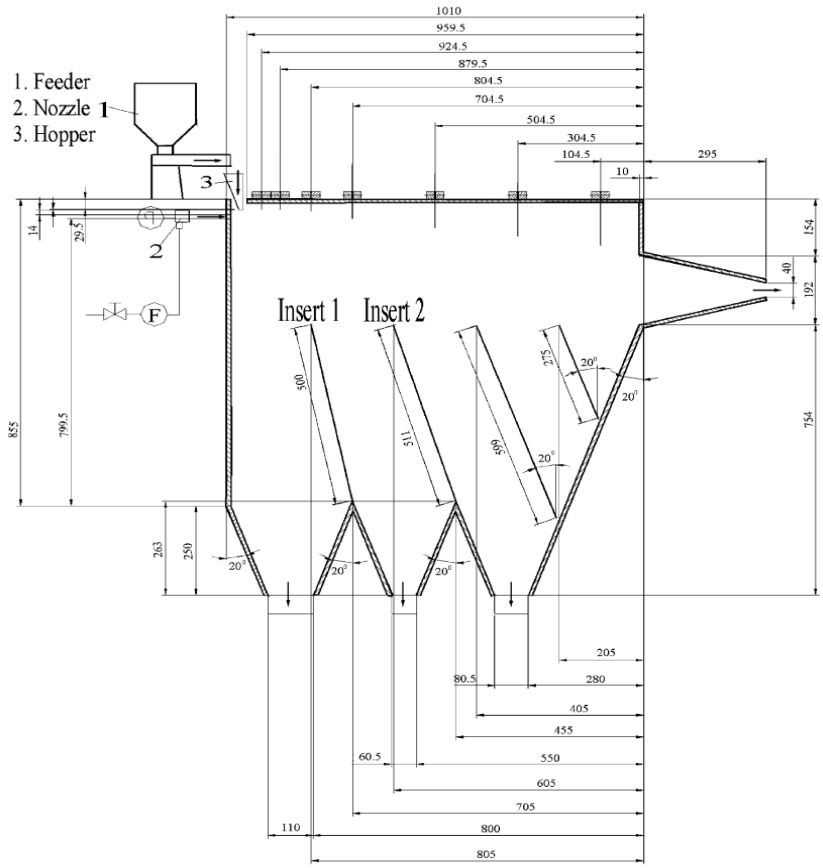

Figure 10: Schematic representation of crossflow classifier with approximate dimensions.

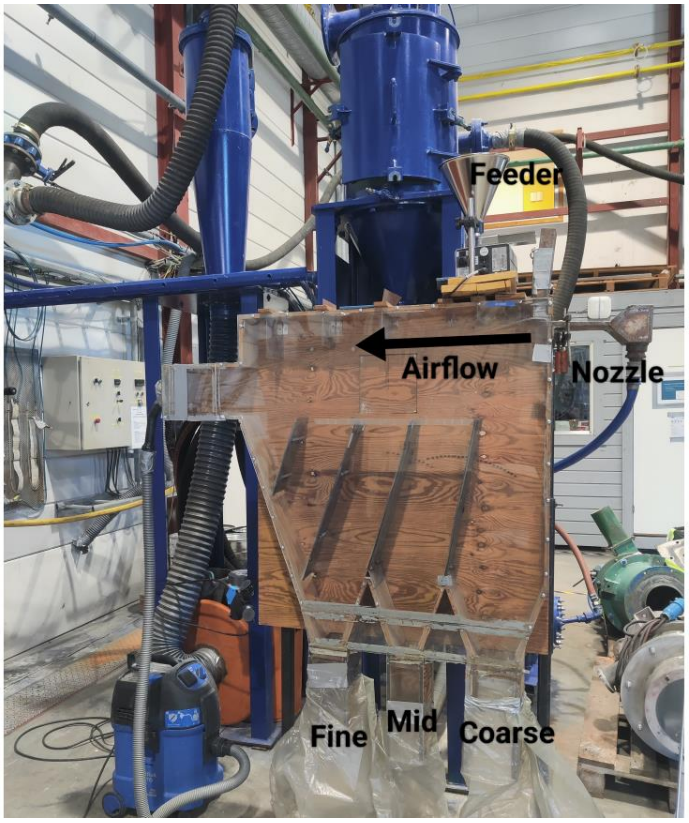

Figure 11: Crossflow air classifier.

Over the past years, SINTEF Tel-Tek (previously known as, dept. of POSTEC under Tel-Tek), has undertaken several research investigations [9] on applications, efficiency enhancement and optimisation of crossflow classifiers, focusing particularly on refining the precision of cut-sizes. These studies have underscored the significant influence of the geometry on the flow field within such classifiers, subsequently impacting the resultant cut-sizes, efficiency, capacity, etc.

When the air flow transitions from a smaller cross-sectional area, such as the nozzle, into a larger area represented by the classifier, the emergence of one or more vortices becomes a distinct possibility. The critical inquiry pertains to the management of these vortices, as they notably affect the finer particles to a greater extent compared to the coarser ones. Initial investigations revolved around evaluating the unit's performance through a combination of experimental analyses and simulation studies [9].

The classifier, along with its accompanying apparatus, is illustrated in Figure 10 and Figure 11. The feed material is introduced through a vibrating feeder (1) and activated hopper (3). The air nozzle (2) propels and directs the particles along different trajectories, with the specific trajectory determined by the interplay of various acting forces on each particle. The feed material undergoes segregation into three fractions facilitated by insert 1 and insert 2, while the remaining two inserts maintain a slight gap between themselves and the wall, allowing the particles to descend through.

Under WP7 in the ReSoURCE project, the evaluation of the crossflow air classifier's performance is cantered on assessing the cut size and sharpness of cut under varying operational conditions and loads, utilizing leftover materials. Through the implementation of sieve analyses and the HELOS-laser method, the behavioural patterns of separation parameters, including cut size, sharpness of cut, grade efficiency curves, and product distributions, have been thoroughly examined. The experimental investigation was carried out as a part of a master’s study in the University of Southeastern Norway (USN) with the supervision of SINTEF research team of ReSoURCE project. The following section provides a brief overview about the experimental method and results.

Materials and Experimental Procedure

For the experiments, the leftover samples from the cement (CRK) and steel (SCL) refractory break out material have been used. The sample materials were pre-sieved into five different particle size ranges; 0-0.25 mm, 0.25- 0.5 mm, 0.5-1 mm, 1-3 mm, and 3-5 mm. A total of 500 g of sample particles from each cement and steel leftovers were used for the classifying procedure imitating the industrial field conditions. The composition of each sample is given in the Table 6.

Table 6: Composition of test samples.

Test Material	Size [mm]				
	0-0.25	0.25-0.50	0.50-1.00	1.00-3.00	3.00-5.00
CRK leftover [g]	70	25	75	235	95
SCL leftover [g]	80	80	90	210	40

The classifier functioned under varying air flow rates and velocities. The air volume flow rates of 40 m^3/h, 60 m^3/h, and 70 m^3/h were used for the tests, and the corresponding air velocities were calculated as 8 m/s, 12 m/s, and 14 m/s respectively since the cross-sectional area of the air inlet was 14 cm^2. The system pressure remained constant at 1 bar, regulated by a barometer to manage the air feed rate. Particles were introduced through a feeder at the top and descended vertically along with the air flow, segregating into three distinct groups that were then gathered at the base using plastic bags, and they were named as 'fine', 'mid' and 'coarse'.

The collected samples were tested for their particle size distributions (PSD) using a sieving tower. In addition to the traditional PSD presentations (graphical, and with key values; d25, D50, d75, etc.), the results were also interpreted in 'Tromp Curve' concept and other relevant performance indices; Sharpness of Separation (SoS), Imperfection Factor (IF), etc, [3].

Results

The findings of cross-flow air classification are presented through conventional particle size distribution curves and Tromp curves. To enhance comprehension of the classifier's efficiency, two Tromp curves are used. Tromp 1 primarily illuminates the effectiveness of separating coarser to mid-range particles, whereas Tromp 2 sheds light on the performance in separating mid-range to finer particles. Together, the combined particle size distribution and the two Tromp curves offer a comprehensive insight into the entire separation process.

Two typical PSD and Tromp curves are given below, while the other curves are provided in Appendix C.

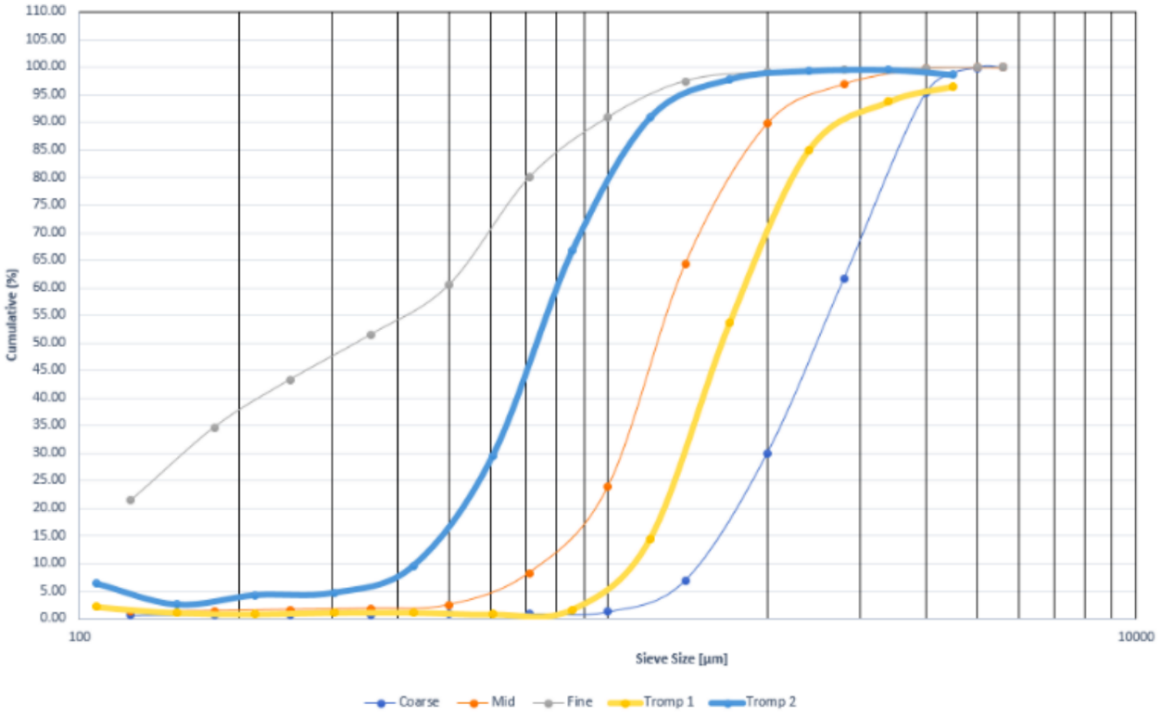

Figure 12 : Results of CRK leftover sample tested under 12m/s air velocity.

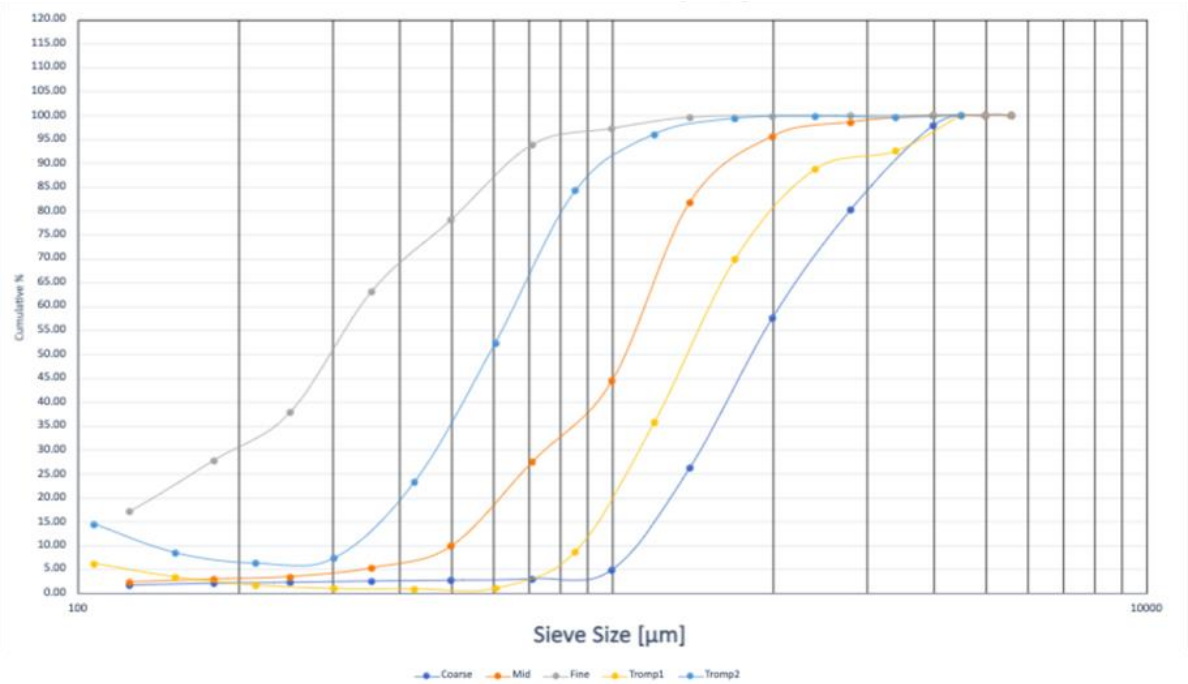

Figure 13: Results of SCL leftover sample tested under 12m/s velocity.

The results are summarised in the

Table 7.

Table 7: Results of cross-flow air classification experiments.

Test Material	Tromp Curve	Parameter	Air Velocity (m/s)		
			8	12	14
CRK leftover	Tromp 1	d25 (µm)	700	1334	1340
		d50 (cut size) (µm)	850	1750	1750
		d75 (µm)	1080	2176	2190
		SoS	1.54	1.63	1.63
		IF	0.22	0.24	0.24
	Tromp 2	d25 (µm)	250	563	510
		d50 (cut size) (µm)	340	740	690
		d75 (µm)	420	973	870
		SoS	1.68	1.73	1.71
		IF	0.25	0.27	0.26
SCL leftover	Tromp 1	d25 (µm)	690	1070	1430
		d50 (cut size) (µm)	860	1400	1900
		d75 (µm)	1130	1820	2600
		SoS	1.64	1.70	1.82
		IF	0.25	0.26	0.31
	Tromp 2	d25 (µm)	260	440	570
		d50 (cut size) (µm)	360	590	750
		d75 (µm)	470	760	990

		SoS	1.81	1.73	1.74
		IF	0.29	0.27	0.28

4.2 Single Column Fluidization

As a first investigation of the fluidization property of a material, a single column is used to investigate fluidization parameters experimentally. In this section the fluidization experiments in a single column will follow.

Materials and Experimental Procedure

A rectangular column was used with dimensions 7 x 20 cm. A picture of the setup is shown in Figure 14. The air supply was split in two inlets, to evenly distribute the air flow over the permeable barrier separating the air feed chamber from the powder material. The permeable barrier was made of SIPERM® R20, stainless steel 37-42 % porosity [10]. Pressure sensors were mounted one at the air inlet chamber, four along the bed column and one by the outlet. The air feed was controlled by three different flow controllers depending on the amount of air needed, 4-150 l/min, 10-300 l/min and 100-1000 l/min.

Before starting an experiment, the material was loaded through the top of the column using a funnel. The weight of the powder was measured, and enough to cover the two lowest pressure sensors. A cap on top of the column was properly sealed with tape after loading the material. A bucket with filters was used to collect fines following the air stream. Samples of the fine fraction were collected directly from the filter bucket. Samples from the coarse fraction were collected from the leftover material in the column after finishing the test.

Figure 14 Experimental setup. Fluidization column with air inlet and pressure sensors. To the right, outlet trough filter bucket.

While running the experiment, the pressure and weight of the filter bucket was logged every second. Adjusting the air flow was done manually. The flow was increased with 2 l/min every 50-100 seconds, when stable pressure was observed. Each step was visually inspected for volume increase, bubbling or channelling in the bed.

Five experiments were carried out in the single column setup, given in Table 8. The same five size fractions as used in the cross-flow experiments were used in the fluidization experiments.

Table 8 Materials used in the single column fluidization experiments.

Material type	Size fraction [mm]	Feed [g]
CRK	0-0.25	3835
CRK	0-5*	4000
SCL	0-0.5 **	3400
SCL	0.25-0.5	2948
CRK	0.25-0.5	3341

* Mixed back to the size distribution as a real industrial case, same mixing ratio as in Table 6.
** 50/50 mix of 0-0.25 mm fraction and 0.25-0.5 mm fraction.

Results

The measured minimum fluidization velocity, U_{mf}, is given in Table 9. The fluidization plots are given in

Figure 15 to Figure 16. The minimum air velocity in the rig is 0.0047 m/s, corresponding to 4 l/min through the 7 x 20 cm area. The smallest fraction of CRK did already bubble at this velocity. The full

mixture of CRK 0-5 mm is not possible to fluidize because of the content of coarse particles. The height of the bed was measured at each step while increasing the flowrate, and the total increase in height after the experiment is given in Table 9. The increase in beg height shows a good air retention property of the material in the smallest size classes.

Table 9 Experimentally measured minimum fluidization velocity, U_{mf}

Material type	**Size fraction [mm]**	**U_{mf} [m/s]**	**Bed height increase**
CRK	0-0.25	<0.0047	NA
CRK	0-5	NA	NA
SCL	0-0.5	0.012	4.5 cm
SCL	0.25-0.5	0.079	0.5 cm
CRK	0.25-0.5	0.043	2 cm

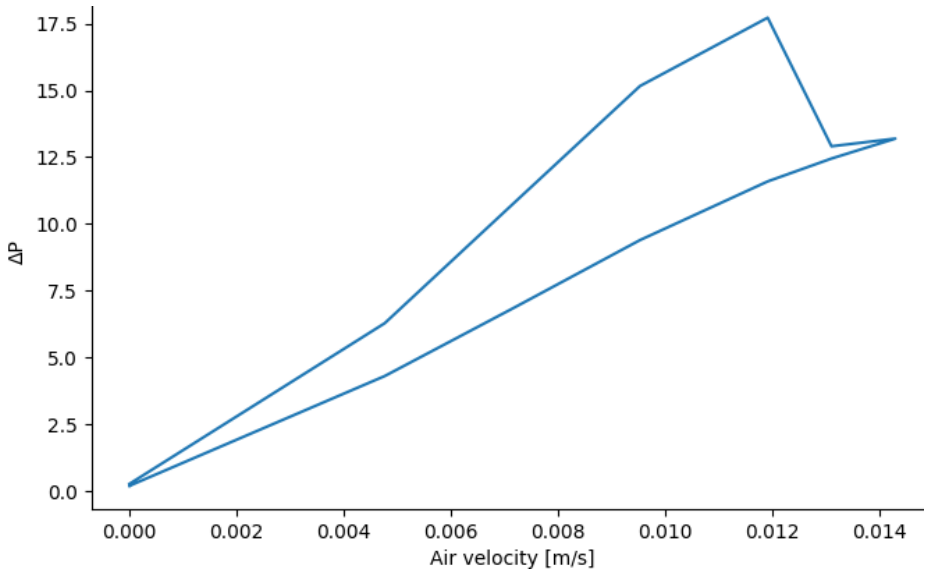

Figure 15 SCL 0-0.5 mm

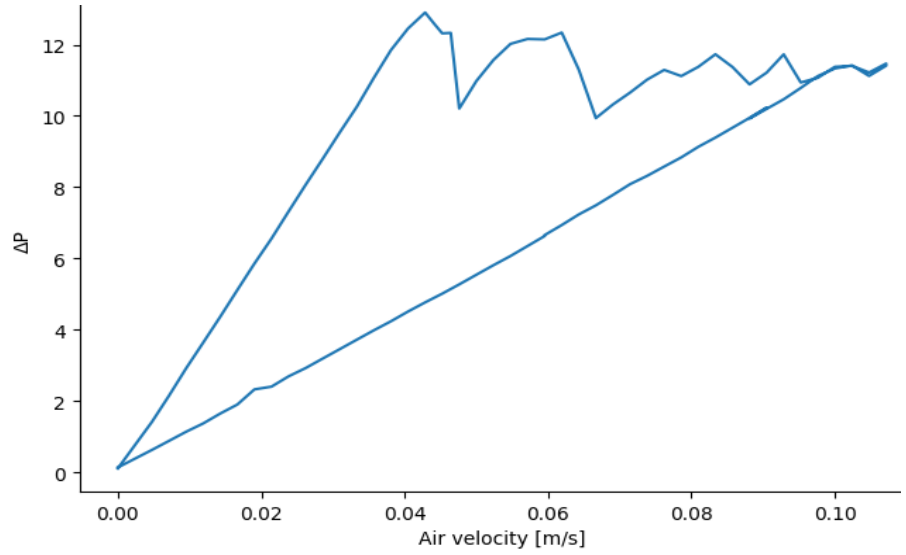

Figure 16 CRK 0.25-0.5 mm

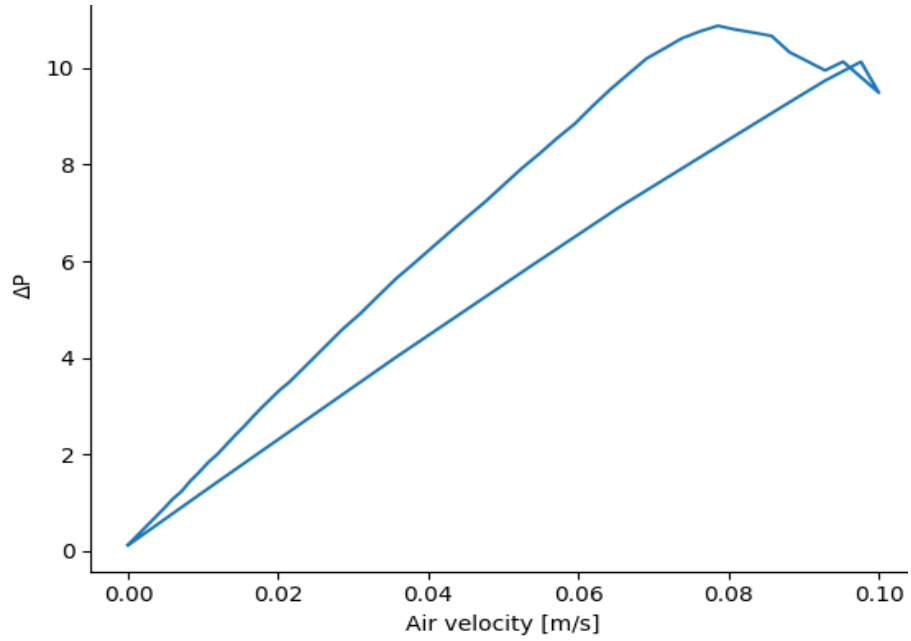

Figure 17 SCL 0.25-0.5 mm

After investigating the minimum fluidization velocity, the flowrate was gradually further increased to separate the feed into a fine and coarse fraction. The fine fraction would follow the air stream into the filter bucket, while the coarse part would be left in the fluidization column. This test was done in two of the experiments, where the maximum air velocity is given in Table 10.

Table 10 Mass balance after separation.

Material type	**Size fraction [mm]**	**Feed [g]**	**Maximum air velocity [m/s]**	**Fine fraction [g]**	**Coarse fraction [g]**
CRK	0-0.25	3835	0.60	1598	1931
SCL	0-0.5 *	3400	0.62	1008	2244

* 50/50 mix of 0-0.25 mm fraction and 0.25-0.5 mm fraction

PSD of the collected fine and coarse fraction is presented in Figure 19 for CRK 0-0.25 mm. The Tromp curve shows a good separation. In Figure 20 the PSD of the fine and coarse fraction of the SCL 0-0.5 mm separation. The PSD was measured on different lenses in the Helos instrument; thus a Tromp curve is not estimated in this experiment.

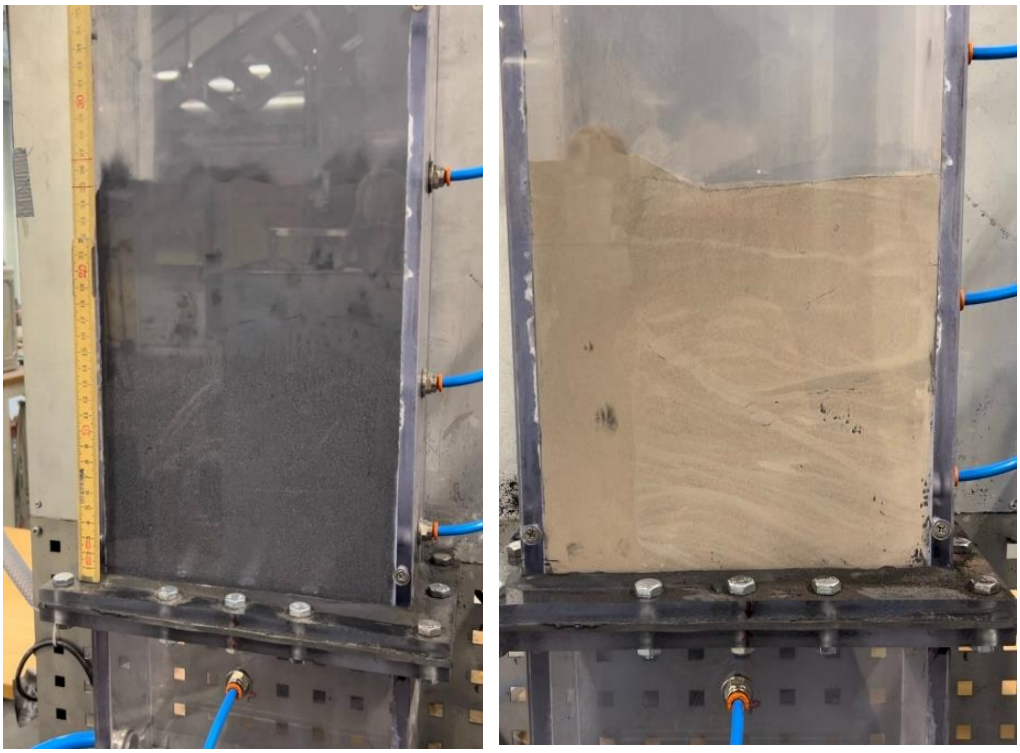

Figure 18 SCL 0-0.5 mm under fluidization experiment at 0.031 m/s visible segregation (left) and 0-0.25 mm CRK at the lowest air velocity. Visible bubbles in the columns left part (right).

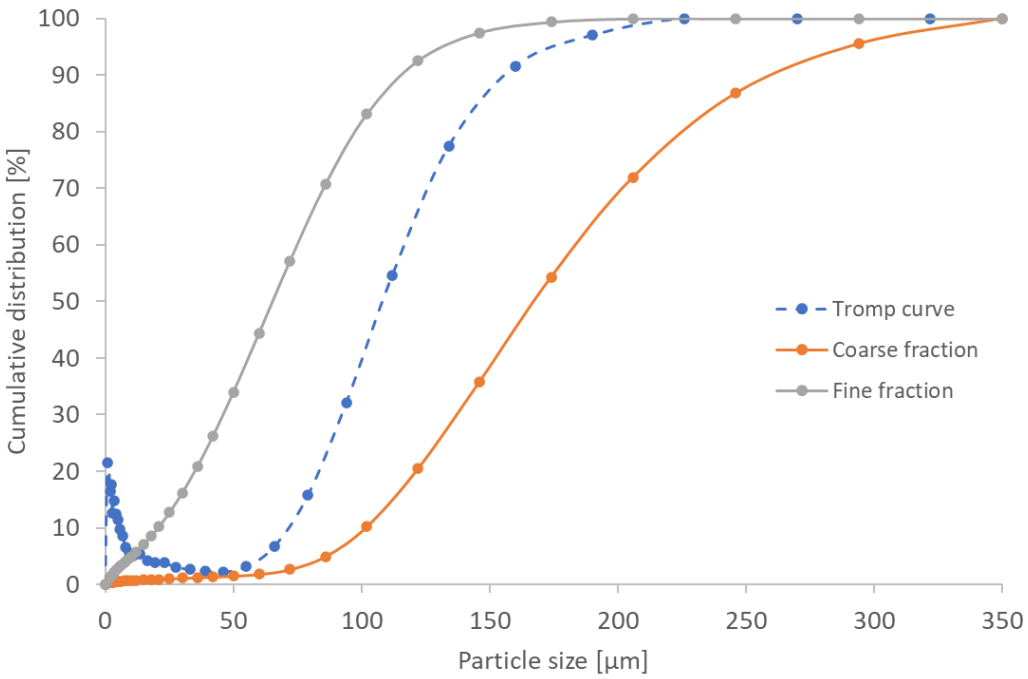

Figure 19 CRK 0-0.25 mm fine and coarse fraction and tromp curve after max air velocity 0.60 m/s.

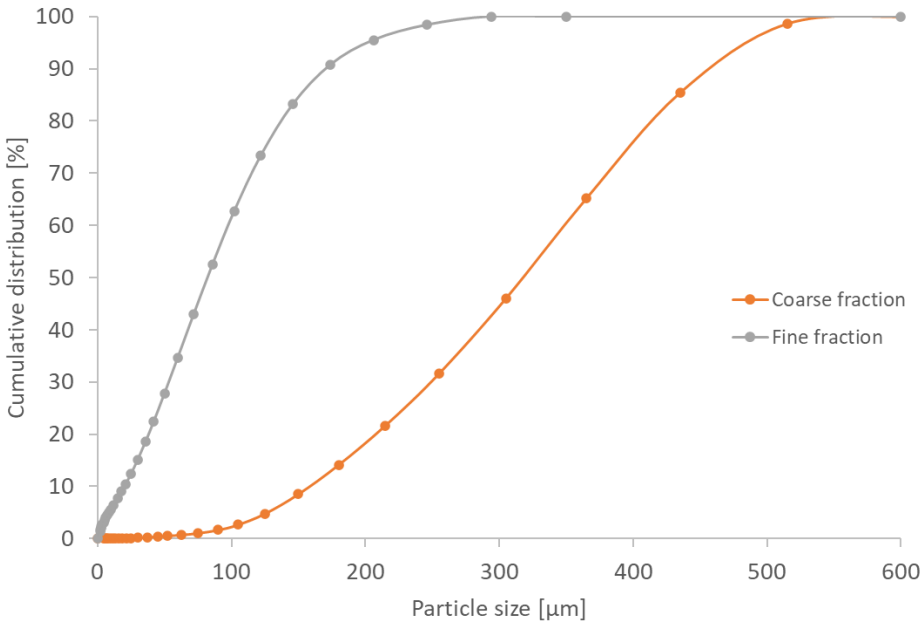

Figure 20 SCL 0-0.5 mm fine and coarse fraction after max air velocity 0.62 m/s.

Figure 21 CRK leftover material 0-5 mm while fluidization experiment at air velocity 0.24 m/s

The mix of CRK 0-5 mm was tested in the fluidization column to see the behaviour if the leftover material, with composition similar to the industrial case, was directly fluidized with no pretreatment. In the picture in Figure 21, a channel has been created to transport the air stream through the material, similar to Geldart's powder group D. The air stream does not mix the material, which makes separation difficult.

The behaviour of the size class 0.25-0.5 mm was more similar to Geldart's powder group B. Especially visible for the SCL material where there was visible big air bubbles slugging. The CRK material had smaller bubbles, and more similar to powder group A or B. Segregation of fine particles was also more visible collected at the top of the powder bed. Pictures of the two 0.25-0.5 mm materials are given in Figure 22.

Figure 22 SCL (left) and CRK (right) both 0.25-0.5 mm at 0.095 m/s.

Conclusion

The smallest size fractions < 5 mm show promising results for use of fluidization as separation technique. Based on the findings in this study, necessary parameters and powder properties experience was collected to continue experiments in the multi chamber fluidization rig.

4.3 Multi Chamber Fluidization

The multi chamber fluidization rig was built by SINTEF (previously named Tel-Tek). The rig was built with the purpose of separating two different particles with difference in density and size. The separation efficiency was reported to 98 %, optimized using Computational Fluid Dynamics simulations. Even if the rig was designed to separate two materials different from refractory, the rig is still suited to separate fine fraction of refractories based on the same principal of difference in size and/or density [11].

A schematic drawing of the rig is shown in Figure 23. The separation unit has five chambers, all with a separate air inlet underneath a permeable membrane of the type SIPERM® R20, stainless steel 37-42% porosity [10], same as used in the single column experiments. A rotary valve is feeding the material into the fluidization chamber, and the air flow will separate the powder, where the light small particles will follow the air flow to a cyclone, while the coarser particles will move vertically and be collected in a collecting tank. A filter was attached after the cyclone and the system was balanced with a suction to avoid an over pressure in the system.

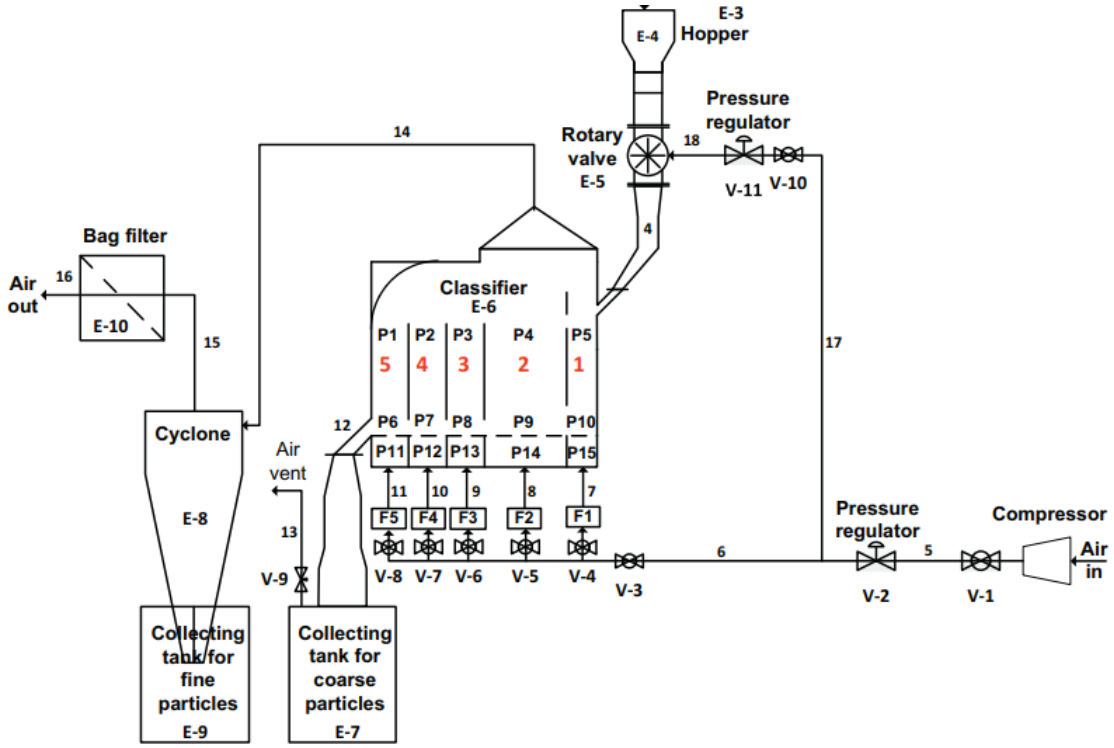

Figure 23 Drawing of the multi chamber rig at SINTEF [12].

The first experiments were carried out with SCL leftover starting with the smallest fraction 0-0.25 mm, then 0-0.5 mm and up to 0-1 mm size. The rig cannot handle coarser particles without changing components in the feeding system. To check the separation efficiency, experiments with pure sintered MgO raw material mixed with graphite raw material were also tested. Using virgin raw material shows a "best case" example where the carbon is not physically bound to MgO particles.

The air velocity in each chamber was set based on previous experiments in the fluidization column and based on the experiments previously carried out using the same rig. An overview of all experiments, materials and air velocities in the chambers are given in Table 11. The weight of each fraction was measured to make a mass balance for each experiment. The rig is made for continuous operations, and thus some material will end up inside the chamber after the experiment. When changing from one material to another, the chamber was dismantled and fully emptied before a new material was introduced. Two samples were collected from the fine and coarse fractions for PSD and chemical analysis. The sampling was done manually mixing the fraction and take out a mixed sample.

Table 11 Experimental setup for multi-chamber fluidization.

			Air velocities [m/s] in given chamber nr.				
Test nr.	**Material**	**Size fraction [mm]**	**1**	**2**	**3**	**4**	**5**
Test 1	SCL	0-0.25	0.2	0.2	0.3	0.35	0.4
Test 2	SCL	0-0.25	0.8	0.7	1.1	1.6	1.7
Test 3	SCL	0-0.25	0.5	0.5	0.7	0.9	1
Test 4	SCL	0-0.25	0.3	0.3	0.5	0.7	0.8
Test 5	SCL	0.25-0.5	0.8	0.7	1.1	1.6	1.7
Test 6	SCL	0.25-0.5	1	1.2	1.4	1.6	1.7
Test 7	SCL	0-0.5	0.6	0.7	0.8	0.9	1

Test 8	SCL	0.5-1	1.1	1.1	1.2	1.4	1.5
Test 9	SCL	0-1	0.6	0.7	0.8	0.9	1
Test 10	CRK	0-0.25	0.2	0.2	0.3	0.35	0.4
Test 11	CRK	0-0.25	0.5	0.5	0.6	0.7	0.8
Test 12	CRK	0-0.5	0.6	0.7	0.8	0.9	1
Test 13	CRK	0-1	0.6	0.7	0.8	0.9	1
Test 14	CRK	0-1	0.4	0.5	0.6	0.7	0.8
Test 15	Sintered MgO and graphite mix	0-1	0.6	0.65	0.7	0.8	0.8
Test 16	Sintered MgO and graphite mix	0-1	0.3	0.3	0.4	0.5	0.6
Test 17	Sintered MgO and graphite mix	0-0.1	0.3	0.3	0.4	0.5	0.55

Results SCL

The mass balance of the SCL experiments (Test 1-9) is presented in Table 12. The negative loss in mass in Test 6 is caused by an increased air velocity from the previous test, thus leftover material left in the chamber followed the product streams. A picture from Test 7 is shown in Figure 24. The light small particles are following the airstream upwards, while the coarser fraction is transported vertically into the collection bucket.

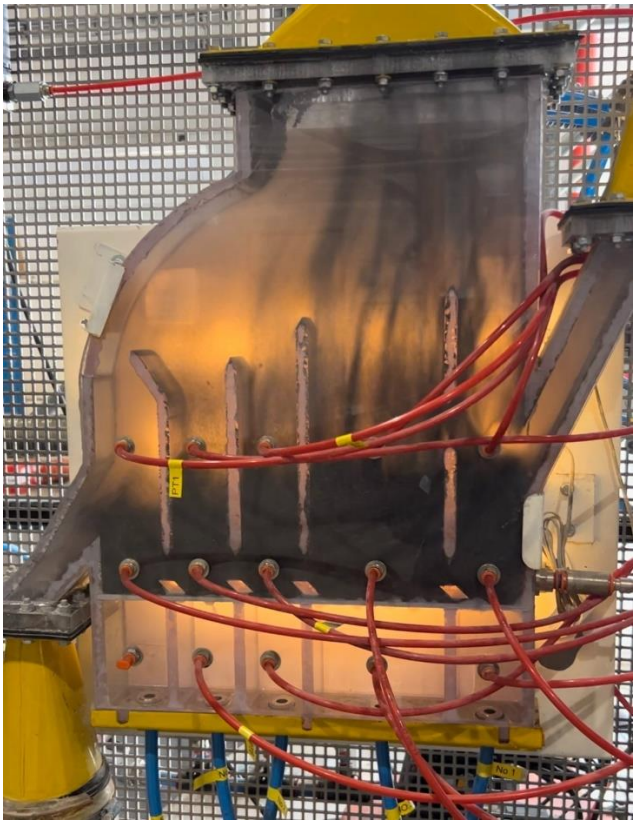

Figure 24 Picture during the separation test 7 with SCL 0-0.5 mm.

Table 12 Mass balance multi-chamber fluidization experiments with SCL leftover material

	Feed [g]	Coarse fraction [g]	Fine fraction [g]	Loss [%]
Test 1	6768	6354	246	2.4
Test 2	6192	1854	4278	0.3
Test 3	4876	2540	2308	0.4
Test 4	3572	2558	926	2.3
Test 5	4624	4328	246	1.1
Test 6	3422	3174	262	-0.4
Test 7	4148[1)]	2564	1382	4.9
Test 8	4860	4332	34	10.2
Test 9	5312[2)]	4192	1080	0.8

1) Mix of 2394 g 0-0.25 mm and 1754 g 0.25-0.5 mm.
2) Mix of 1714 g 0-0.25 mm, 1716 g 0.25-0.5 mm and 1882 g 0.5-1 mm.

The particle size distribution in the product fractions from Test nr. 1-9 is presented in Table 13. Test 1 and 4 has still some fine fraction in the coarse product, with X10 at 35 and 28 µm respectively. These tests have the lowest air velocities, while higher velocities show a better removal of fine particles. In test 9 the mix of leftover SCL 0-1 mm was tested. The PSD plot of fine and coarse fraction is presented in Figure 25. The Tromp curve shows a good separation of the fine particles below ca. 230 µm.

Table 13 PSD of SCL fine and coarse fraction after multi-chamber fluidization classifier.

		X10 [µm]	X16 [µm]	X50 [µm]	X84 [µm]	X90 [µm]
Test 1	Fine	13.7 ± 0.4	19.9 ± 0.5	52 ± 0.7	119.2 ± 1.6	148.7 ± 2.4
	Coarse	34.6 ± 0.7	54 ± 0.8	131.6 ± 1.8	216.1 ± 2.8	237.1 ± 2.3
Test 2	Fine	30.2 ± 0.4	45.2 ± 0.7	113.2 ± 1.7	200.4 ± 1.8	225.9 ± 1.7
	Coarse	110.2 ± 1.6	131.2 ± 1.7	205.1 ± 1.9	282.6 ± 1.3	302.4 ± 1.6
Test 3	Fine	21.8 ± 0.1	32.7 ± 0.1	85.8 ± 0.9	163 ± 1.8	189.8 ± 2
	Coarse	101.1 ± 0.3	120.5 ± 0.2	191.6 ± 0.4	272.3 ± 0.3	291.8 ± 0.1
Test 4	Fine	16.5 ± 0.4	24.4 ± 0.4	63.3 ± 0.7	121.8 ± 1.1	144.5 ± 0.9
	Coarse	28 ± 0.1	44.9 ± 0.4	122.7 ± 1	212.8 ± 1.6	235.4 ± 1.2
Test 5	Fine	70.7 ± 3.7	107.9 ± 7.2	266.3 ± 5.9	379 ± 8.4	410.4 ± 7.7
	Coarse	255.5 ± 2.5	277.1 ± 2.9	375.6 ± 5.9	495.3 ± 10.3	529.5 ± 21.3
Test 6	Fine	115.3 ± 7.8	174.2 ± 5.6	293.4 ± 3	395.4 ± 4.6	419.9 ± 4.2
	Coarse	281.6 ± 2.6	310.7 ± 2.3	422.9 ± 3.4	564.7 ± 4.7	600.8 ± 3.9
Test 7	Fine	40 ± 0.3	50.8 ± 0.2	100.3 ± 1.4	175.1 ± 1.2	203.1 ± 0.5
	Coarse	159.4 ± 5.1	185.7 ± 6.6	305.7 ± 13.5	453 ± 25.2	498.1 ± 30.2
Test 8	Fine	42.1 ± 0.3	57.1 ± 0.1	128 ± 0.5	228.2 ± 2.8	263.4 ± 6.4
	Coarse	508.7 ± 5.8	555.3 ± 4.9	766.8 ± 8.7	1016.3 ± 23.1	1094.2 ± 43.8
Test 9	Fine	42.7 ± 0.4	54.7 ± 0.6	110.4 ± 1.4	196.2 ± 3.6	229.5 ± 5.9
	Coarse	227.6 ± 2.5	270 ± 3.1	499.5 ± 6	836.2 ± 20.9	944 ± 37.2

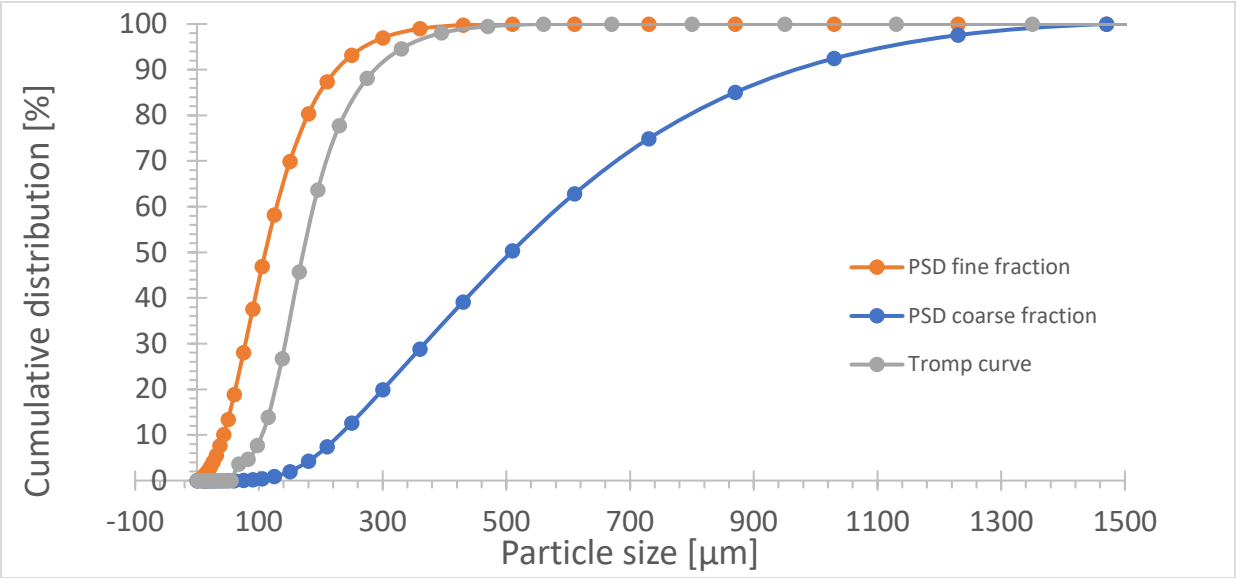

Figure 25 PSD and Tromp curves for test 9 of SCL 0-1 mm.

The total carbon content was analysed for both fractions for each test. The results will be used to optimize the separation in upcoming experiments. There was achieved up to three times higher carbon content in the fine fraction compared to the coarse fraction for some of the experiments.

Results CRK

The mass balance of the CRK experiments (Test 10-14) is presented in Table 14. The negative loss in mass in Test 11 is caused by an increased air velocity from the previous test, thus leftover material inside the chamber followed the product streams.

Table 14 Mass balance multi-chamber fluidization experiments with CRK leftover material.

	Feed [g]	Coarse fraction [g]	Fine fraction [g]	Loss [g]	Loss %
Test 10	3552	2768	395	389	11.0
Test 11	3378	2102	1580	-304	-9.0
Test 12	3282[1)]	1674	1446	162	4.9
Test 13	4134[2)]	2554	1174	406	9.8
Test 14	3084[3)]	2244	700	140	4.5

1) Mix of 2044 g 0-0.25 mm and 1238 g 0.25-0.5 mm.
2) Mix of 1690 g 0-0.25, 684 g 0.25-0.5 mm and 1760 g 0.5-1 mm.
3) Mix of 1278 g 0-0.25, 476 g 0.25-0.5 mm and 1330 g 0.5-1 mm.

The particle size distribution in the product fractions from Test nr. 10-14 is presented in Table 15. The PSD analysis shows a successful reduction of the smallest particles in the coarse fraction after separation. The PSD plot of fine and coarse fraction from Test 14 is presented in Figure 26. The Tromp curve shows a good separation of the fine particles below ca. 130 µm.

Table 15 PSD of fine and coarse fraction of CRK experiments in multi-chamber fluidization classifier.

Test nr.	Fraction	X10 [µm]	X16 [µm]	X50 [µm]	X84 [µm]	X90 [µm]
Test 10	Fine	8.2 ± 0.8	12 ± 0.8	31.4 ± 0.7	57.1 ± 0.9	66.6 ± 1.3
	Coarse	45 ± 0.9	58.9 ± 1.2	122 ± 2	203.4 ± 1.6	227.6 ± 1.5
Test 11	Fine	17.6 ± 0.1	25.4 ± 0.1	60.4 ± 0.1	106.6 ± 0.4	121.9 ± 0.7

	Coarse	82.6 ± 1.3	96.3 ± 1.4	153.8 ± 1.6	222.1 ± 1.1	239.6 ± 0.6
	Fine	21.6 ± 0.2	31.5 ± 0.3	78 ± 0.6	137.1 ± 0.9	157.4 ± 1.2
Test 12	Coarse	136.7 ± 0.7	157.4 ± 0.7	262.4 ± 2.3	426.3 ± 10.9	476.8 ± 16.5
	Fine	20.9 ± 0.1	30.7 ± 0.3	77.7 ± 0.8	137.7 ± 2	157.7 ± 3.5
Test 13	Coarse	165.9 ± 0.9	198 ± 1.7	475.1 ± 14.2	969.5 ± 31.7	1102.6 ± 51.4
	Fine	17.7 ± 0.2	26.3 ± 0.2	65.3 ± 0.3	111.8 ± 1	125.7 ± 1.5
Test 14	Coarse	134.3 ± 0.4	158.9 ± 0.7	406.8 ± 7	919.6 ± 10.6	1043.9 ± 17.6

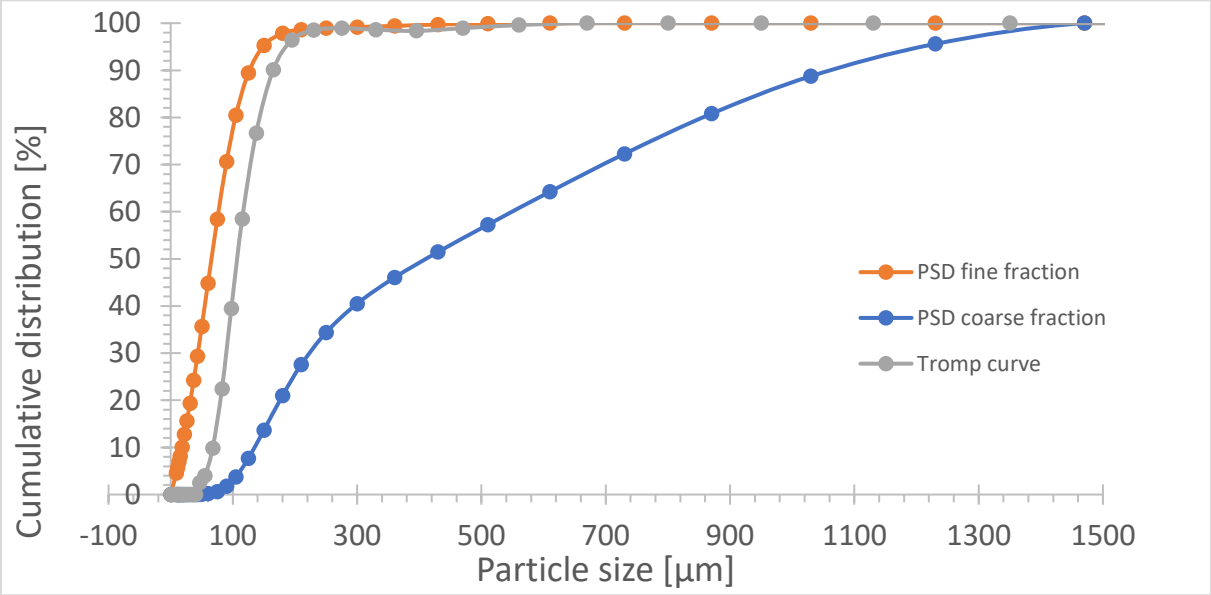

Figure 26 PSD and Tromp curves for test 14 after multi-chamber fluidization classification with CRK 0-1 mm

Separation of MgO and graphite raw material

In test number 15-17 raw material of sintered MgO and graphite were mixed and fed into the multi-chamber rig to investigate the separation when the two phases were not physically bound to each other. Two tests were conducted with MgO particles of 0-1 mm and one with 0-0.1 mm size. The graphite raw material was the same in each test and had an X90 = 256 µm. Experimental setup is shown in Table 16.

Table 16 Air velocities used in the multi-chamber rig with sintered MgO and graphite raw material.

		Velocity [m/s] in chamber nr.				
Test nr.	**Particle size of MgO [mm]**	**1**	**2**	**3**	**4**	**5**
Test 15	0-1	0.6	0.65	0.7	0.8	0.8
Test 16	0-1	0.3	0.3	0.4	0.5	0.6
Test 17	0-0.1	0.3	0.3	0.4	0.5	0.55

The fluidization chamber was first filled with sintered MgO and fluidized with the highest air velocity of the test to achieve a stable layer of MgO in the rig. In this way, the calculated loss in the system after introducing the test material was reduced. The mass balance of the experiments is given in Table 17. The loss is still considerably high, but the small sample size and trapped material inside the rig

explains the main part. Small amounts of material was collected in the filter, but were not measured because of the neglectable amount.

Table 17 Mass balance of the experiments with MgO and graphite raw material.

	Feed MgO [g]	Feed Graphite [g]	Coarse fraction [g]	Fine fraction [g]	Loss [%]
Test 15	1002	300	670	370	20.1
Test 16	900	200	350	256	44.9
Test 17	716	236	292	484	18.5

During the experiments, there was a clear visual difference in colour of the output to the coarse fraction and the fine fraction. A picture of the rig is shown in Figure 27 and the fine and coarse fraction outputs are shown in Figure 28. The colour diffraction visualizes the potential difference in carbon content. Also, the particle size distribution in Table 18 confirms the low content in carbon. The coarse fraction in Test 15 and 16 has an X10 above or close to the graphite X90 particle size, which indicates that only the 10% coarsest particles of carbon can be present in the coarse fraction after separation.

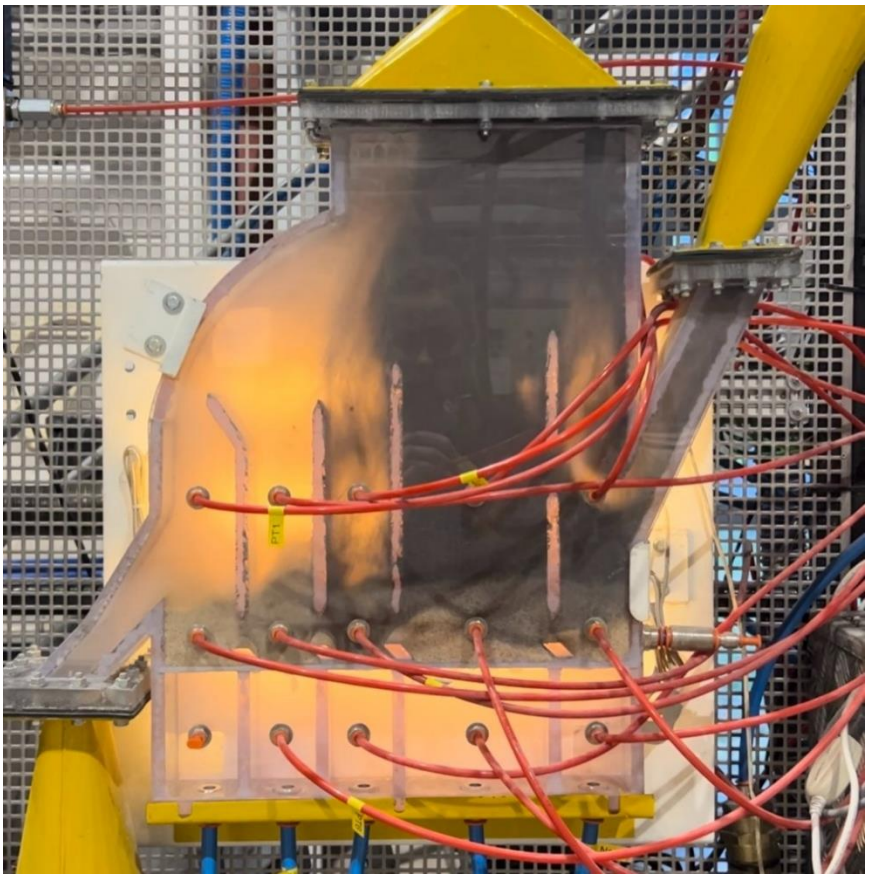

Figure 27 Mix of sintered MgO raw material 0-1 mm and graphite raw material.

Figure 28 Fine (left) and coarse (right) fraction after separation in Test 15.

Table 18 PSD of product fractions after separation of sintered MgO and graphite raw material in multi-chamber fluidization classifier.

Test nr.	Fraction	x10 [µm]	x16 [µm]	x50 [µm]	x84 [µm]	x90 [µm]
Test 15	Fine	18 ± 0.1	27.3 ± 0.1	86.8 ± 0.6	191.9 ± 0.2	227.3 ± 0.9
	Coarse	298.9 ± 5.6	378.1 ± 7.5	680.3 ± 19.3	967.4 ± 32	1033.5 ± 39.2
Test 16	Fine	18 ± 0.1	27.3 ± 0.1	86.8 ± 0.6	191.9 ± 0.2	227.3 ± 0.9
	Coarse	206.2 ± 0.8	255.8 ± 1.5	588.1 ± 13.8	971.6 ± 46	1074.7 ± 61.6
Test 17	Fine	8.8 ± 0.2	14.9 ± 0.4	60.8 ± 1.6	156.8 ± 5.4	194.5 ± 7.9
	Coarse	12.6 ± 0.1	24.9 ± 0.1	120.7 ± 0.6	262.5 ± 2.3	304 ± 2.9

4.4 Alternative Separation Processes

There are several separation techniques that have been evaluated for the leftover material. At the Chair of Mineral Processing at Montanuniversitaet Leoben, there are four processes which seem to be suitable to produce separate refractory fines utilizing different properties of the powders:

- Sieve set
- Air separation table (dry process) and lab shaking table (wet process)
- Corona drum separator
- Flotation

The processes needs to be experimentally tested to evaluate the output fractions, potential for optimizing and use as a pretreatment process. The methods utilize different principles for separation. Sieving separates the material based on the grain size with a mesh in different sizes determine the cut size. The air separation table uses the principle of fluidization to separate the particles based on density, shape and mass. In the corona drum separator, the conductivity of the materials in the different particles determines the separation. Flotation is a wet process that utilizes the surface properties of the particles for separation. Surface active chemicals in addition to an air stream creating bubbles, provides a bubble-particle interaction where particles with different surface characteristics

can be separated. A more detailed description of the separation processes is described in Appendix D. The separation methods will be tested in and reported in deliverable D7.2 and D7.3.

5. Conclusion and further work

Fluidization has shown promising results for use as dedusting technique before further handling and recycling of the leftover refractory <1 mm. Enriched content of carbon in the finest SCL fraction indicates that the same technique can be used to reduce the content of carbon while removing the dust fraction. Findings from the classification experiments will be used in the development of demonstrator B in WP8.

To verify the findings in this report, material from other origins will be tested. The material in this report is from one casting ladle and one cement rotary kiln, new samples from other steel casting ladles and rotary kilns will be provided for upcoming experiments to verify the results.

To further optimize the separation method, more experiments with MgO and graphite raw materials will be used to find the optimal conditions for separation with fluidization. Also crushed material within the same size fractions will be experimentally tested to investigate if there is any difference in behaviour from the leftover fraction.

Other separation methods will also be investigated as presented in section 4.4. To find the most efficient and suitable separation method, or combination of separation methods to achieve the desired product fractions.

6. References

[1] M. Shapiro and V. Galperin, 'Air classification of solid particles: a review', *Chem. Eng. Process. Process Intensif.*, vol. 44, no. 2, pp. 279–285, Feb. 2005, doi: 10.1016/j.cep.2004.02.022.

[2] S. P. Gundupalli, S. Hait, and A. Thakur, 'A review on automated sorting of source-separated municipal solid waste for recycling', *Waste Manag.*, vol. 60, pp. 56–74, Feb. 2017, doi: 10.1016/j.wasman.2016.09.015.

[3] B. A. Wills and J. Finch, *Wills' mineral processing technology: an introduction to the practical aspects of ore treatment and mineral recovery*. Butterworth-Heinemann, 2015.

[4] T. J. Napier-Munn, S. Morrell, R. D. Morrison, and T. Kojovic, 'Mineral comminution circuits: their operation and optimisation', 1996.

[5] T. k. Belhaj, M. G. Higazy, A. M. Gaafer, and B. A. K. ELMogy, 'Improvement of Productivity Using Tromp Curve Measurement for Cement Separator Processing Technology', *Sci. J. Oct. 6 Univ.*, vol. 3, no. 2, pp. 35–44, 2016, doi: 10.21608/sjou.2016.31761.

[6] D. Geldart, 'Types of gas fluidization', *Powder Technol.*, vol. 7 (5), pp. 285–292, 1973.

[7] R. Cocco and J. W. Chew, '50 years of Geldart classification', *Powder Technol.*, vol. 428, p. 118861, Oct. 2023, doi: 10.1016/j.powtec.2023.118861.

[8] 'Fluidized beds overview : Fundamentals of fluidized beds design'. Accessed: Nov. 06, 2023. [Online]. Available: https://powderprocess.net/Spray_Drying/Introduction_Fluidized_Beds.html

[9] Q. Wang, M. C. Melaaen, and S. R. De Silva, 'Investigation and simulation of a cross-flow air classifier', *Powder Technol.*, vol. 120, no. 3, pp. 273–280, Oct. 2001.

[10] 'SIPERM® HIGH POROUS SINTERED MATERIALS'. Tridelta Siperm. [Online]. Available: https://www.siperm.com/wp-content/uploads/2020/05/Katalog-en.pdf

[11] C. K. Jayarathna, M. Balfe, B. E. Moldestad, and L.-A. Tokheim, 'Comparison of Experimental Results from Operating a Novel Fluidized Bed Classifier with CFD Simulations Applying Different Drag Models and Model Validation', *Processes*, vol. 10, no. 9, p. 1855, Sep. 2022, doi: 10.3390/pr10091855.

[12] C. K. Jayarathna, M. Balfe, B. M. E. Moldestad, and L.-A. Tokheim, 'Improved multi-stage cross-flow fluidized bed classifier', *Powder Technol.*, vol. 342, pp. 621–629, Jan. 2019, doi: 10.1016/j.powtec.2018.10.026.

[13] P. Schmidt, R. Körber, M. Coppers (2003). Sieving and screening machines: basics and application. Wiley VCH.

[14] M. Lehner (2016). Mechanical Process Engineering, winter semester 2022. Montanuniversitaet Leoben, Chair of Process Engineering for Industrial Environmental Protection.

[15] H. Kirchberg (1953). Processing of mining raw materials. Wilhelm Gronau.

[16] W. Rommel (2004). Practical instructions for fluid bed separator. Augsburg University of Applied Sciences.

[17] H. Schubert (1996). Preparation of Solid Materials: Sorting Processes (4th Edition). German publisher for basic industry.

[18] Hamos GmbH (2023). Operating instructions, electrostatic corona drum separator type KWS-L.

Appendix

A PSD plots CRK and SCL leftover in pre-sieved fractions

HELOS (H1223) & RODOS, R5: 0.5/4.5...875µm **2023-10-09, 16:57:53**,928
Refractory cement

x_{10} = **26.69 µm**	x_{50} = **109.97 µm**	x_{90} = **230.64 µm**	**SMD** = **41.59 µm**	**VMD** = **121.20 µm**
x_{16} = 40.23 µm	x_{84} = 202.63 µm	x_{99} = 345.87 µm	S_V = 0.14 m²/cm³	S_m = 360.62 cm²/g

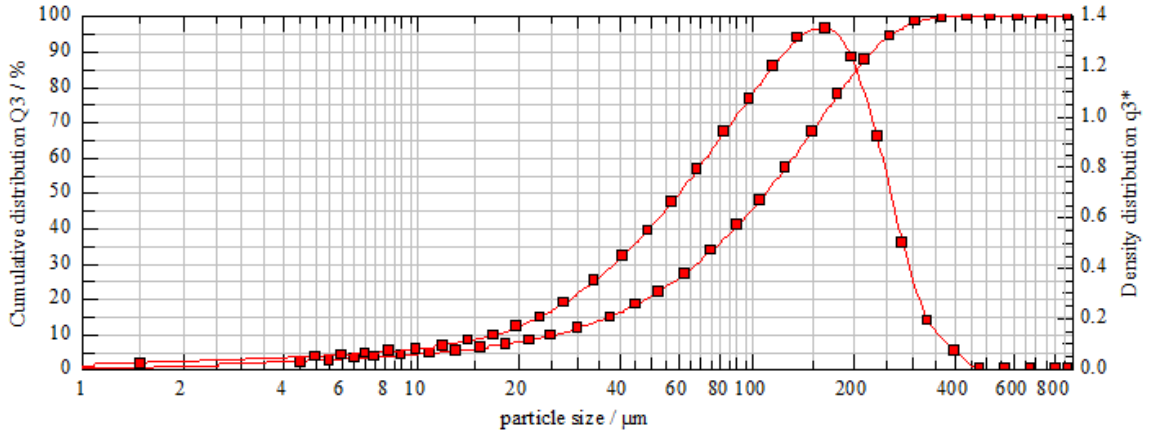

comment:

user parameters:
P1: Test # multichamber ref.
P2: Feed CRK 0. - 0.25 mm 1.2
P3: FOvH

HELOS (H1223) & RODOS, R5: 0.5/4.5...875µm **2023-10-09, 16:12:07**,368
Refractory steel

x_{10} = **171.70 µm**	x_{50} = **340.74 µm**	x_{90} = **501.12 µm**	**SMD** = **245.89 µm**	**VMD** = **338.97 µm**
x_{16} = 217.45 µm	x_{84} = 467.39 µm	x_{99} = 614.00 µm	S_V = 0.02 m²/cm³	S_m = 61.00 cm²/g

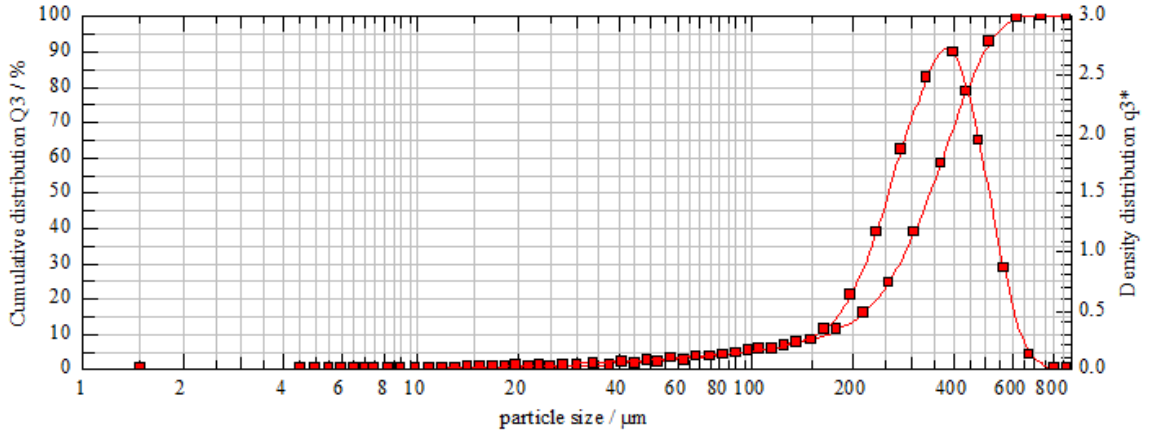

comment:

user parameters:
P1: Test # multichamber ref.
P2: Feed CRK 0.25 - 0.5 mm 1.1
P3: (GRADIS) FOvH

HELOS (H1223) & RODOS, R6: 0.5/9.0...1750µm **2023-10-09, 16:08:26,791**
Refractory steel

x_{10} = 533.53 µm	**x_{50} = 818.44 µm**	**x_{90} = 1161.17 µm**	**SMD = 762.07 µm**	**VMD = 833.15 µm**
x_{16} = 586.39 µm	x_{84} = 1092.15 µm	x_{99} = 1410.24 µm	S_V = 0.01 m²/cm³	S_m = 19.68 cm²/g

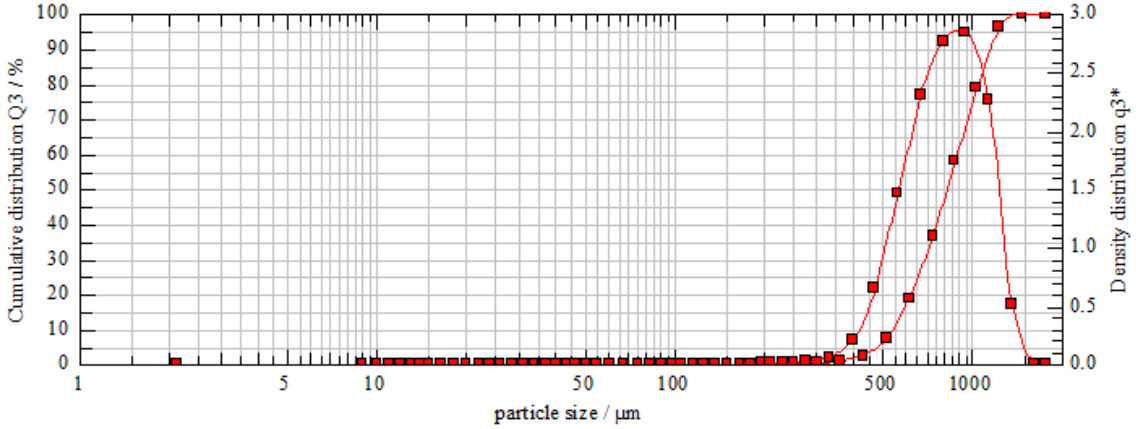

comment:

user parameters:
P1: Test # multichamber ref.
P2: Feed CRK 0.5 - 1.0 mm 1.3
P3: (GRADIS) FOvH

HELOS (H1223) & RODOS, R4: 0.5/1.8...350µm **2023-09-19, 10:48:58,419**
Refractory steel
WARNING: Coarse particles probably exceeding the measuring range.

x_{10} = 27.79 µm	**x_{50} = 123.69 µm**	**x_{90} = 233.68 µm**	**SMD = 36.06 µm**	**VMD = 127.79 µm**
x_{16} = 44.79 µm	x_{84} = 210.97 µm	x_{99} = 286.89 µm	S_V = 0.17 m²/cm³	S_m = 416.01 cm²/g

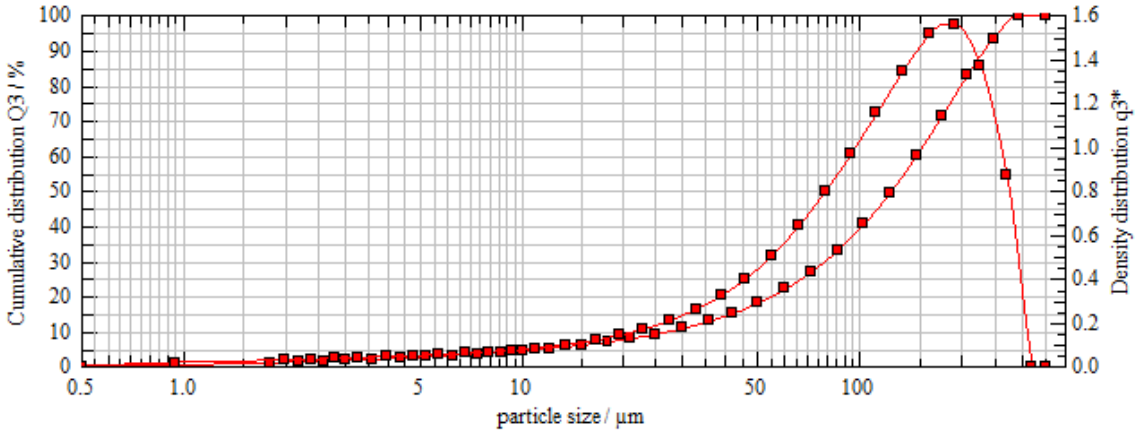

comment:

user parameters:
P1: Test # multichamber feed
P2: Feed 0 - 0.25 mm Referanse 1.2
P3: FOvH

HELOS (H1223) & RODOS, R6: 0.5/9.0...1750µm **2023-10-09, 15:35:20**,049
Refractory steel

x_{10} = 269.66 µm	**x_{50} = 410.74 µm**	**x_{90} = 595.10 µm**	**SMD = 381.44 µm**	**VMD = 426.57 µm**
x_{16} = 300.28 µm	x_{84} = 554.36 µm	x_{99} = 861.51 µm	S_V = 0.02 m²/cm³	S_m = 39.32 cm²/g

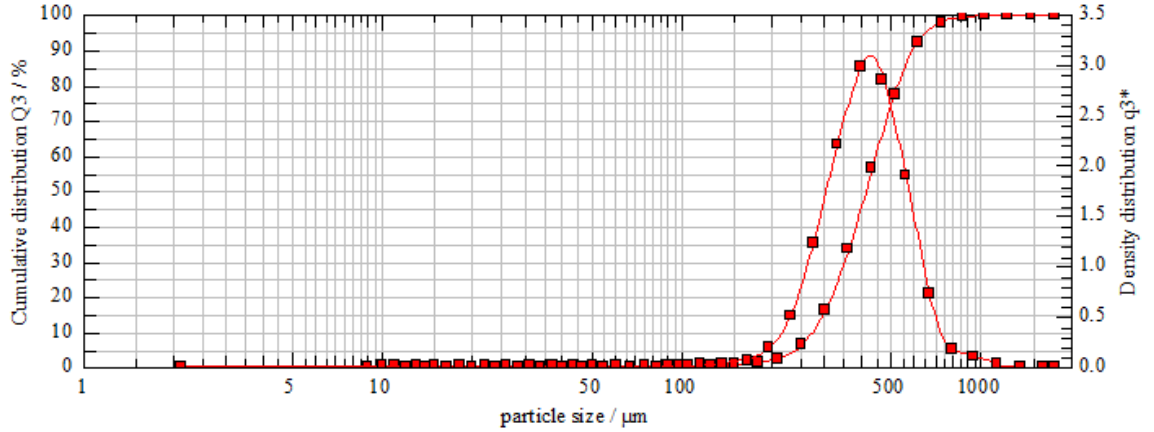

comment:

user parameters:
P1: Test # multichamber ref.
P2: Feed SCL 0.25 - 0.5 mm 1.2
P3: (GRADIS) FOvH

HELOS (H1223) & RODOS, R6: 0.5/9.0...1750µm **2023-10-09, 15:24:19**,511
Refractory steel

x_{10} = 533.76 µm	**x_{50} = 806.69 µm**	**x_{90} = 1144.59 µm**	**SMD = 756.53 µm**	**VMD = 822.49 µm**
x_{16} = 585.42 µm	x_{84} = 1069.50 µm	x_{99} = 1394.41 µm	S_V = 0.01 m²/cm³	S_m = 19.83 cm²/g

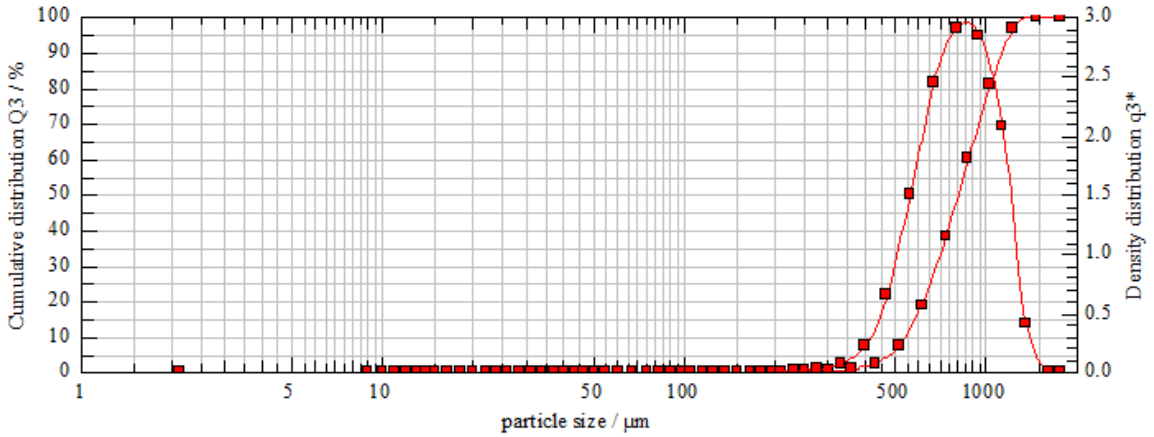

comment:

user parameters:
P1: Test # multichamber ref.
P2: Feed SCL 0.5 - 1.0 mm 1.3
P3: (GRADIS) FOvH

B Shape analysis

Sympatec GmbH
System | Partikel | Technik

SCL 0 - 0.25mm
2023-11-01 09:33:50

SPHERICITY DISTRIBUTION PAQXOS 4.2 **EQPC**, sphere(EQPC), ISO

$s_{10,3}$ = 0.717	$s_{50,3}$ = 0.824	$s_{90,3}$ = 0.887	$Ø_s$ = 0.811	C_{opt} = 0.19 %
$s_{16,3}$ = 0.749	$s_{84,3}$ = 0.875	$s_{99,3}$ = 0.927	σ_s = 0.074	Part. = 5506828

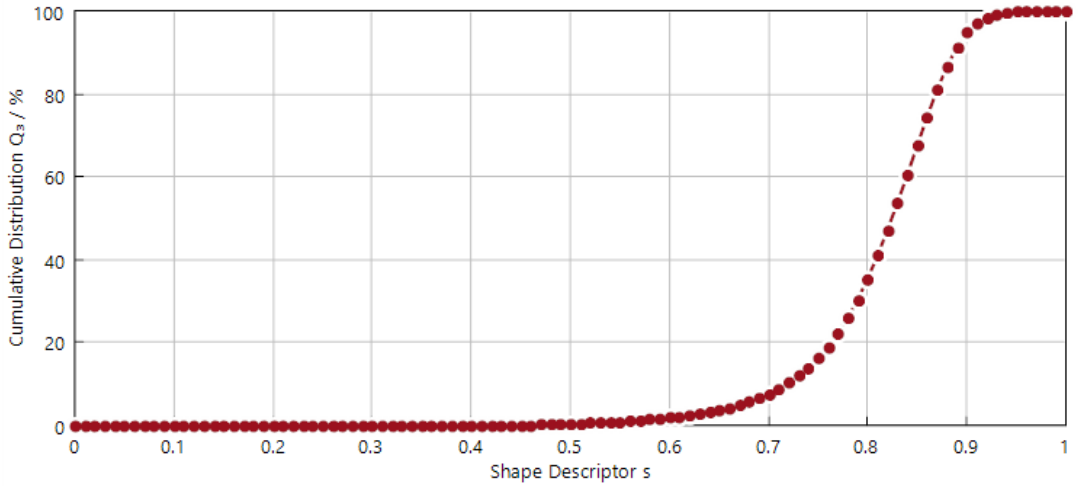

Sympatec GmbH
System | Partikel | Technik

SCL 0.25 - 0.5mm
2023-11-01 09:08:48

SPHERICITY DISTRIBUTION PAQXOS 4.2 **EQPC**, sphere(EQPC), ISO

$s_{10,3}$ = 0.728	$s_{50,3}$ = 0.804	$s_{90,3}$ = 0.860	$Ø_s$ = 0.797	C_{opt} = 0.15 %
$s_{16,3}$ = 0.747	$s_{84,3}$ = 0.849	$s_{99,3}$ = 0.895	σ_s = 0.057	Part. = 981362

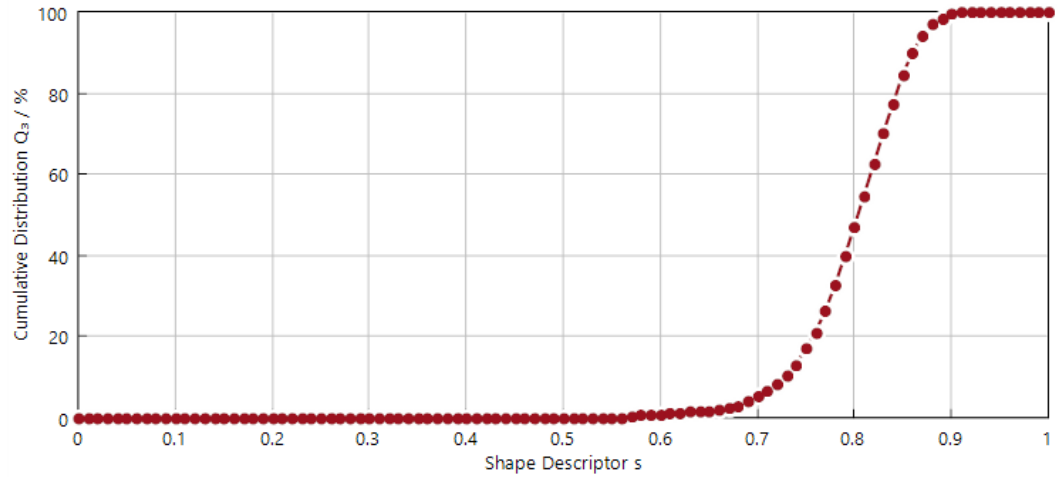

Sympatec GmbH
System | Partikel | Technik

SCL 0.5 - 1mm
2023-10-31 15:32:27

SPHERICITY DISTRIBUTION PAQXOS 4.2 **EQPC**, sphere(EQPC), ISO

$s_{10,3}$ = 0.731	$s_{50,3}$ = 0.798	$s_{90,3}$ = 0.856	$Ø_s$ = 0.795	C_{opt} = 0.08 %
$s_{16,3}$ = 0.751	$s_{84,3}$ = 0.843	$s_{99,3}$ = 0.891	σ_s = 0.050	Part. = 317543

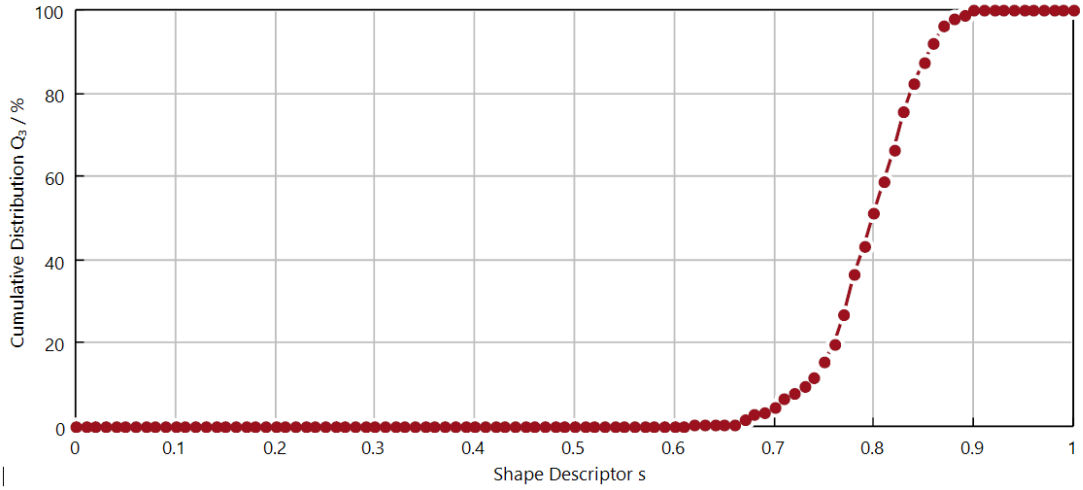

Sympatec GmbH
System | Partikel | Technik

CRK 0 - 0.25mm
2023-10-31 14:44:53

SPHERICITY DISTRIBUTION PAQXOS 4.2 **EQPC**, sphere(EQPC), ISO

$s_{10,3}$ = 0.743	$s_{50,3}$ = 0.847	$s_{90,3}$ = 0.901	$Ø_s$ = 0.831	C_{opt} = 0.25 %
$s_{16,3}$ = 0.776	$s_{84,3}$ = 0.891	$s_{99,3}$ = 0.935	σ_s = 0.075	Part. = 4760716

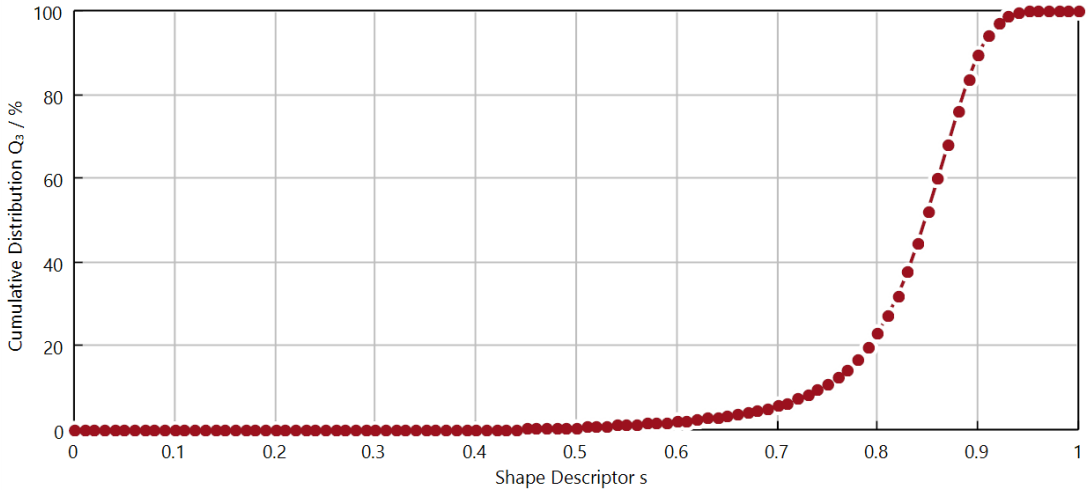

Sympatec GmbH
System | Partikel | Technik

CRK 0.25 - 0.5mm

2023-10-31 14:58:51

SPHERICITY DISTRIBUTION PAQXOS 4.2 **EQPC**, sphere(EQPC), ISO

$s_{10,3}$ = 0.752	$s_{50,3}$ = 0.818	$s_{90,3}$ = 0.866	$Ø_s$ = 0.812	C_{opt} = 0.13 %
$s_{16,3}$ = 0.769	$s_{84,3}$ = 0.857	$s_{99,3}$ = 0.900	σ_s = 0.051	Part. = 520964

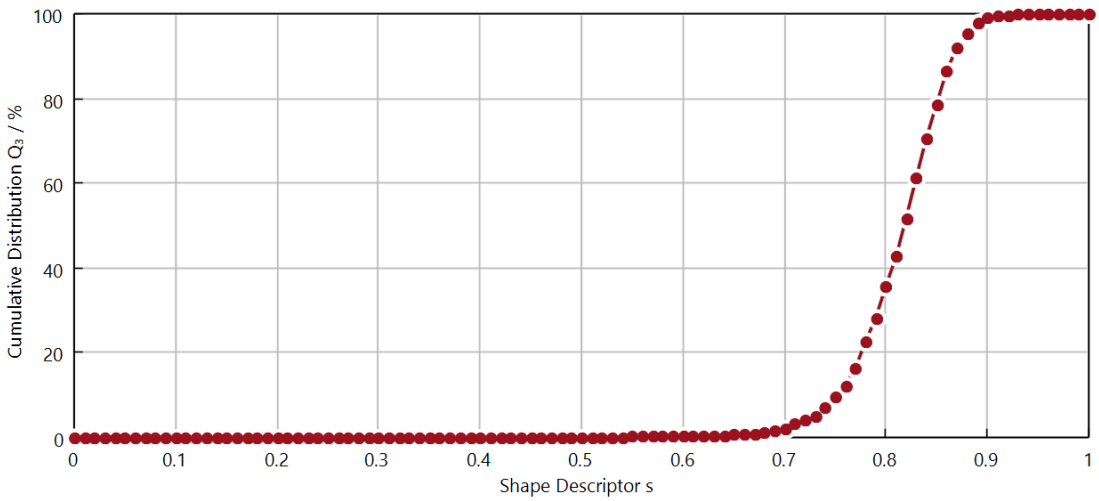

Sympatec GmbH
System | Partikel | Technik

CRK 0.5 - 1mm

2023-10-31 15:18:23

SPHERICITY DISTRIBUTION PAQXOS 4.2 **EQPC**, sphere(EQPC), ISO

$s_{10,3}$ = 0.746	$s_{50,3}$ = 0.810	$s_{90,3}$ = 0.854	$Ø_s$ = 0.803	C_{opt} = 0.09 %
$s_{16,3}$ = 0.762	$s_{84,3}$ = 0.846	$s_{99,3}$ = 0.877	σ_s = 0.046	Part. = 229127

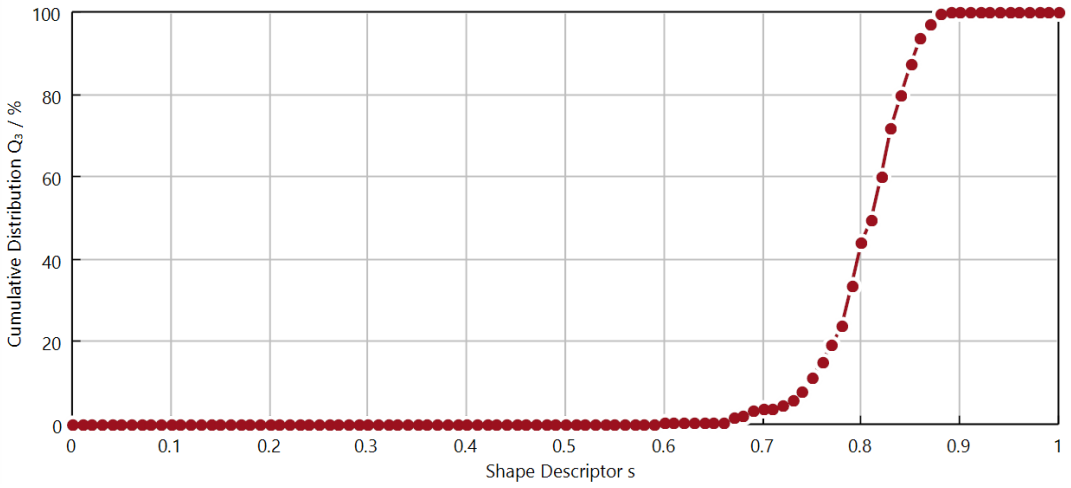

C Cross-flow Air Classification PSD curves

PSD and Tromp curves for CRK 0-5 mm at 8, 12 and 14 m/s air velocity:

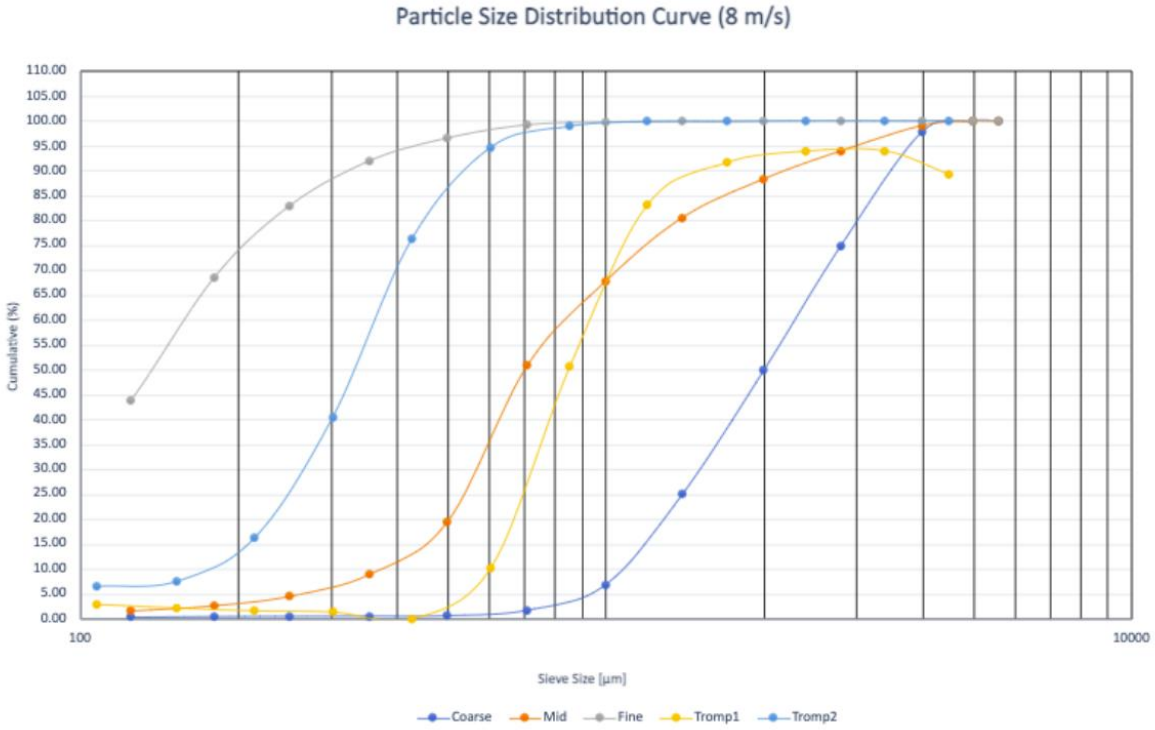

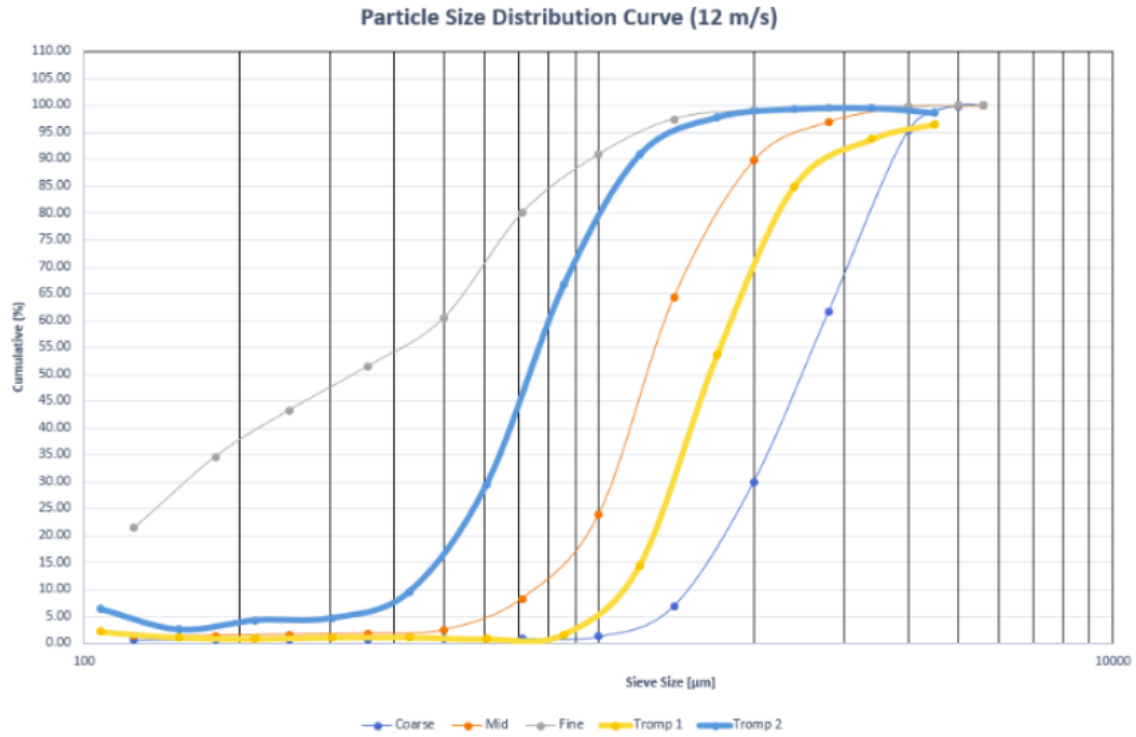

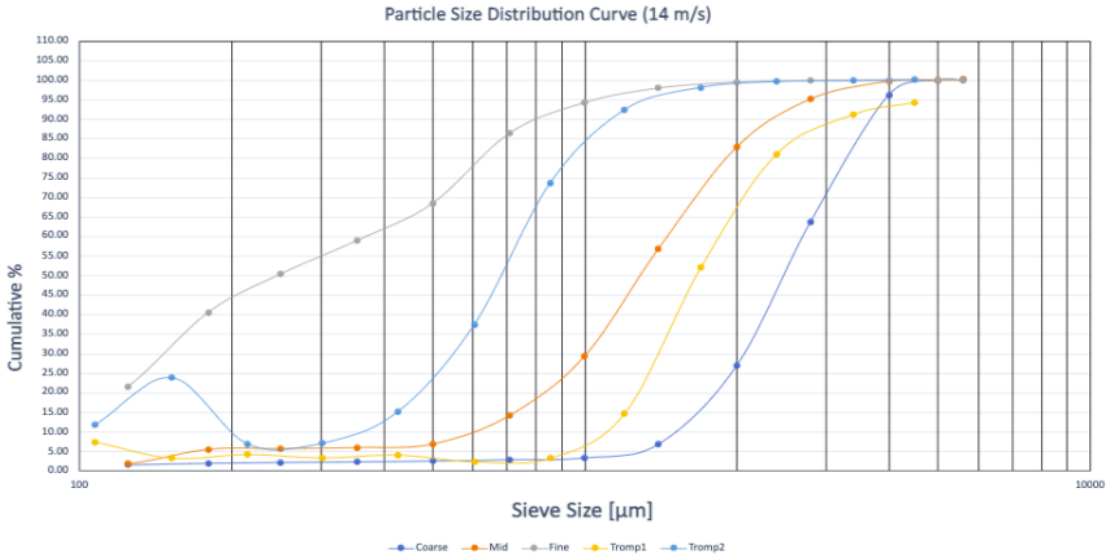

PSD and Tromp curves for SCL 0-5 mm at air velocities 8, 12 and 14 m/s:

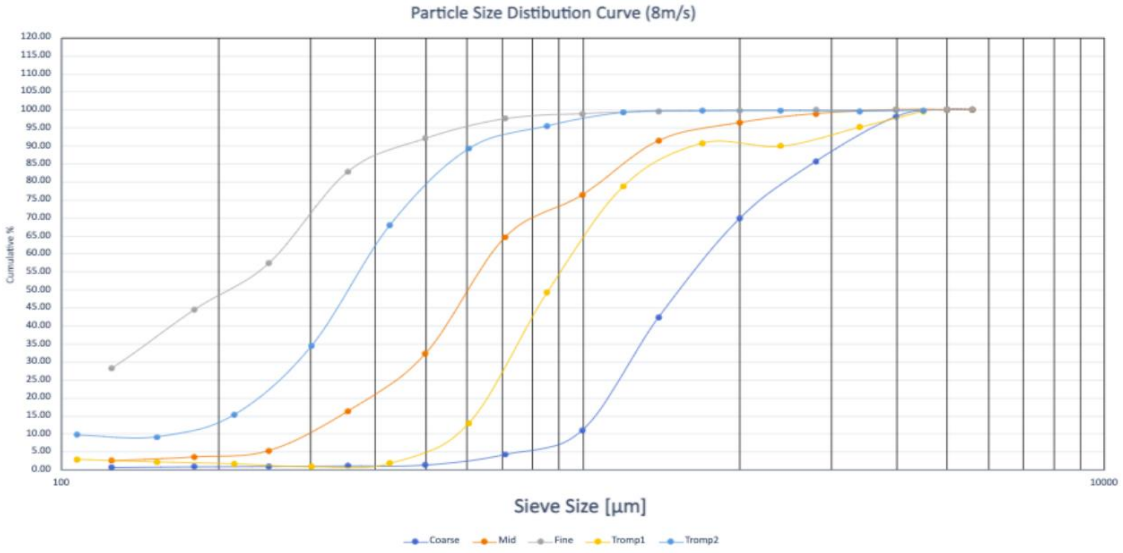

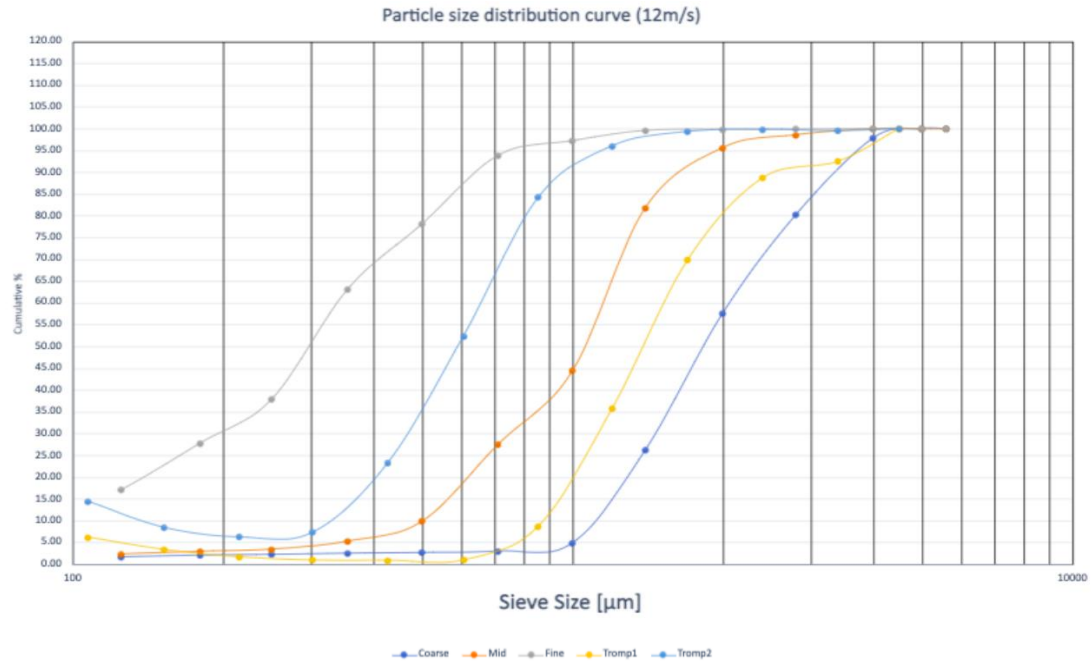
Particle size distribution curve (12m/s)
Cumulative %
Sieve Size [µm]
100
10000
Coarse
Mid
Fine
Tromp1
Tromp2

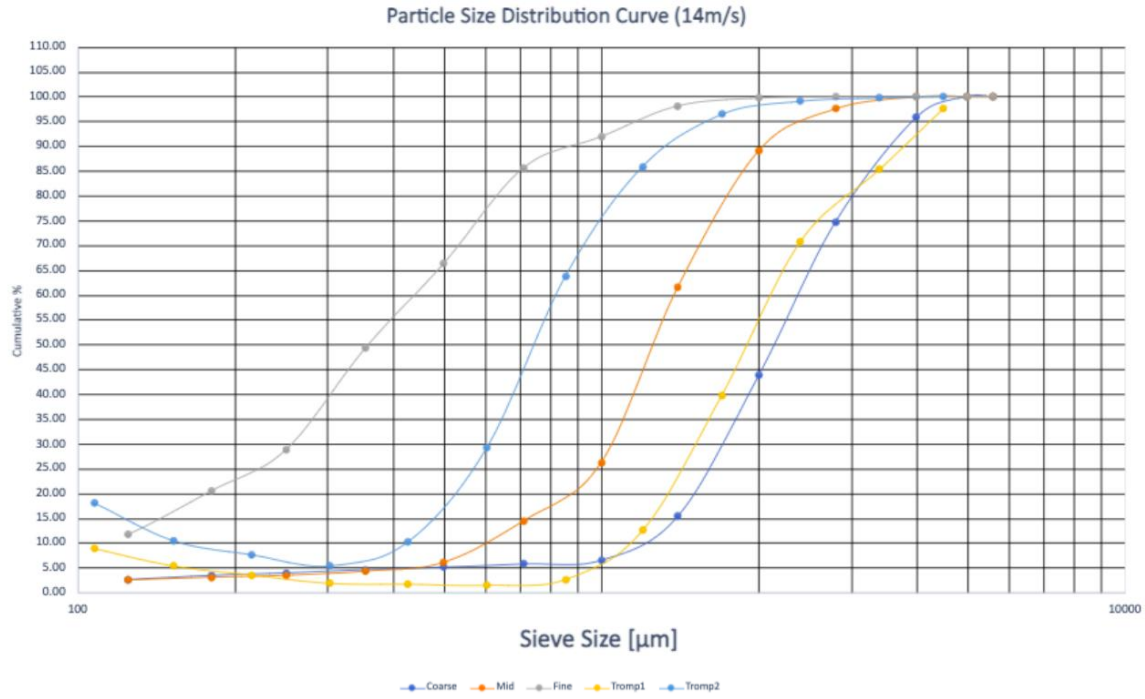
Particle Size Distribution Curve (14m/s)
Cumulative %
Sieve Size [µm]
100
10000
Coarse
Mid
Fine
Tromp1
Tromp2

PSD and Tromp curves for CRK 1-3 mm at air velocities 8, 12 and 14 m/s:

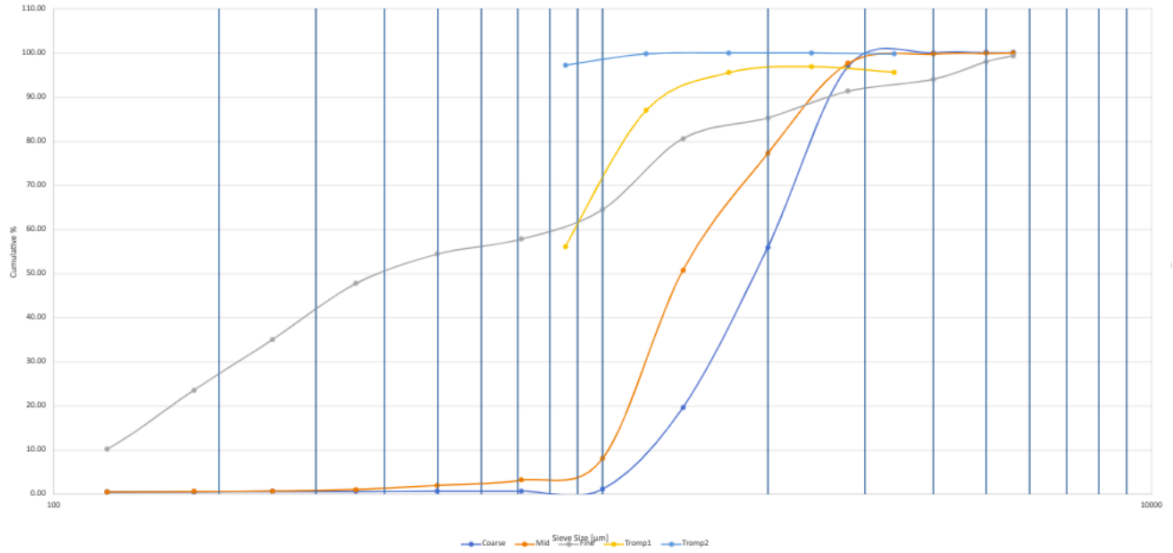

Figure 29 PSD and Tromp curves 1-3 mm at 8 m/s

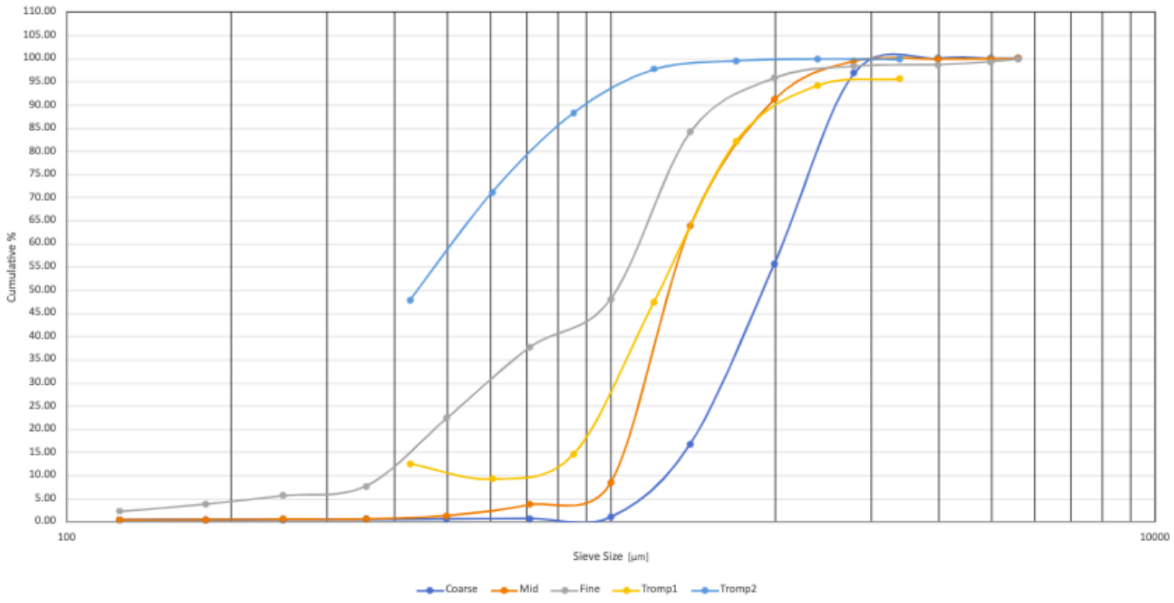

Figure 30 PSD and Tromp curved 1-3 mm CRK at 12 m/s

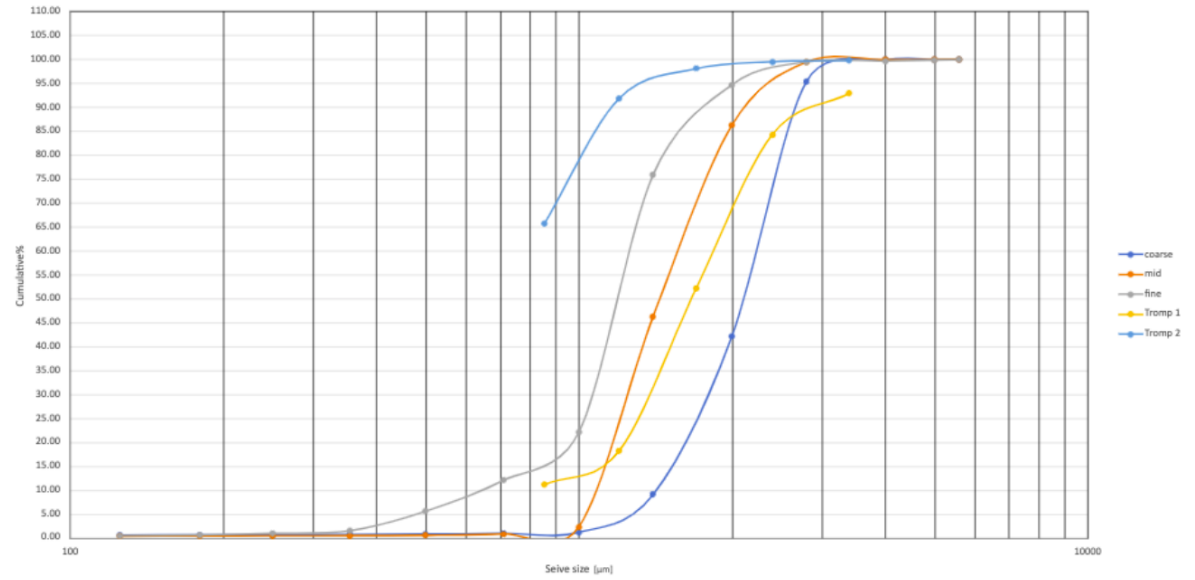

Figure 31 PSD and Tromp curves 1-3 mm CRK at 14 m/s

PSD and Tromp curves for CRK 0.5-1 mm at air velocities 8, 12 and 14 m/s:

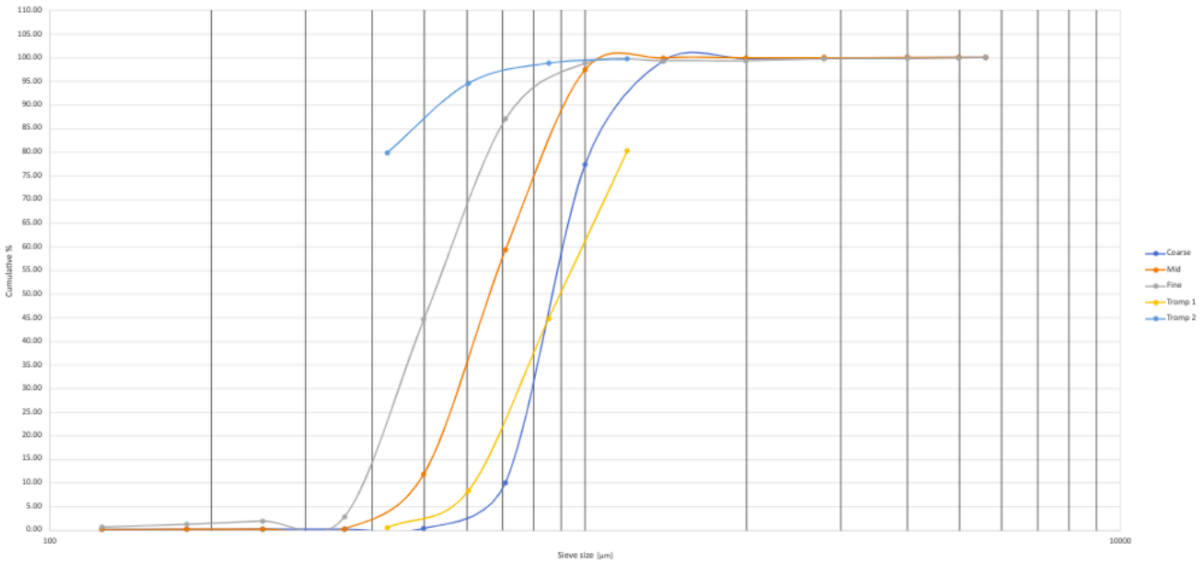

Figure 32 PSD and Tromp curve 0.5-1 mm CRK at 8 m/s

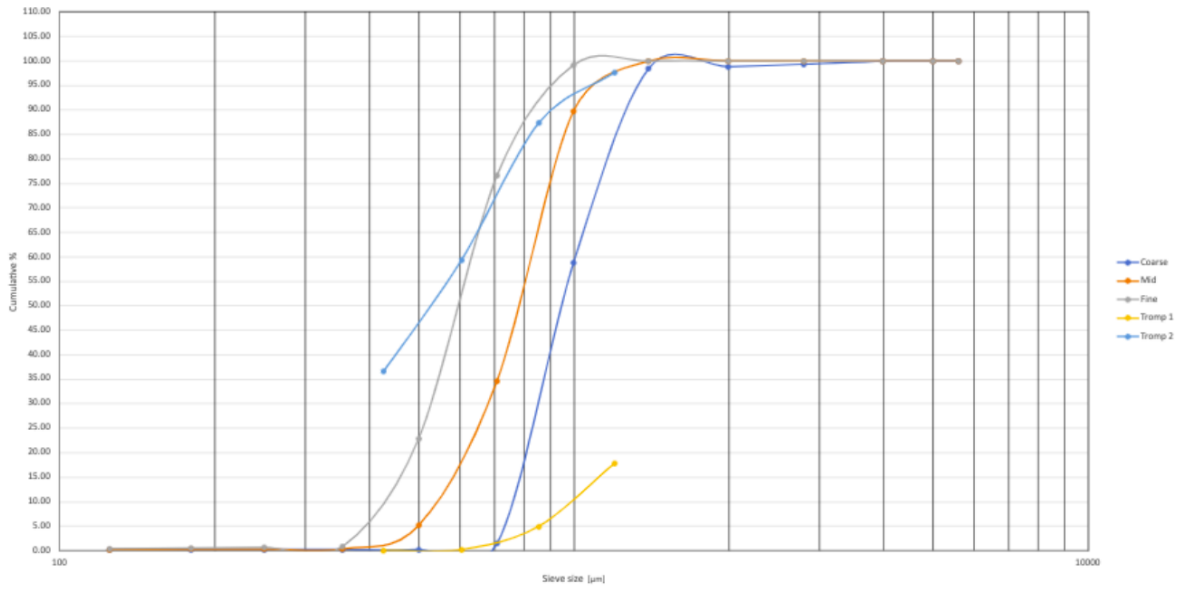

Figure 33 PSD and Tromp curves 0.5-1 mm CRK at 12 m/s

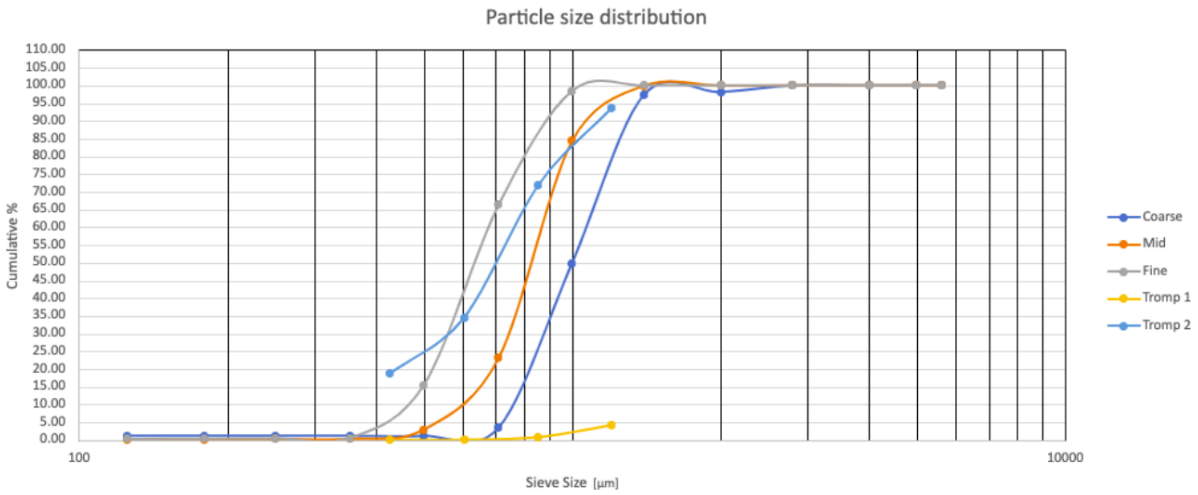

Figure 34 PSD and Tromp curves 0.5-1 mm CRK at 14 m/s

PSD and Tromp curves for SCL 0.5-1 mm at air velocities 8, 12 and 14 m/s:

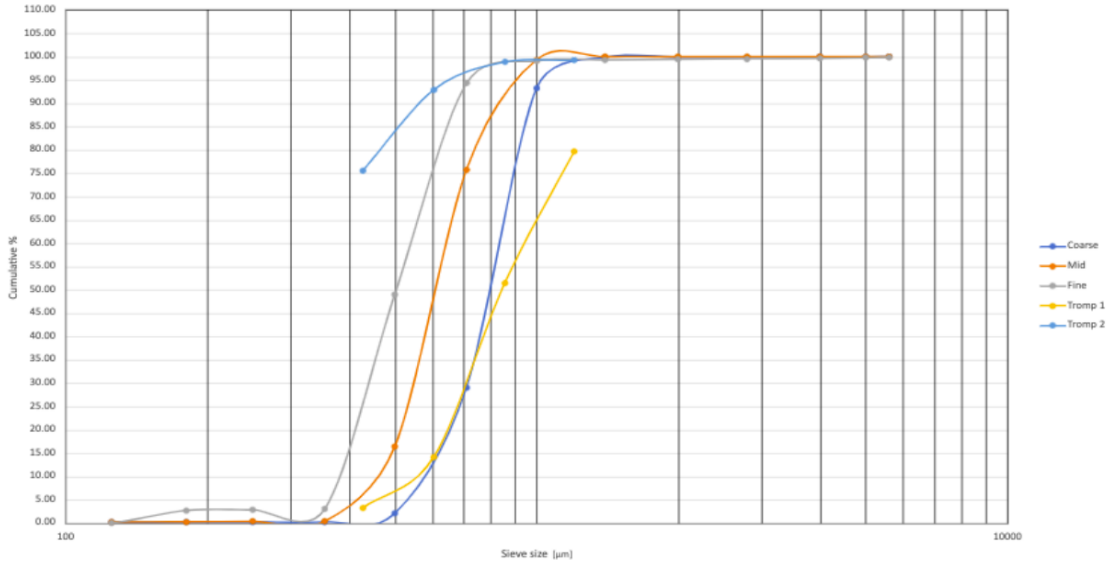

Figure 35 PSD and Tromp Curves 0.5-1mm at 8 m/s

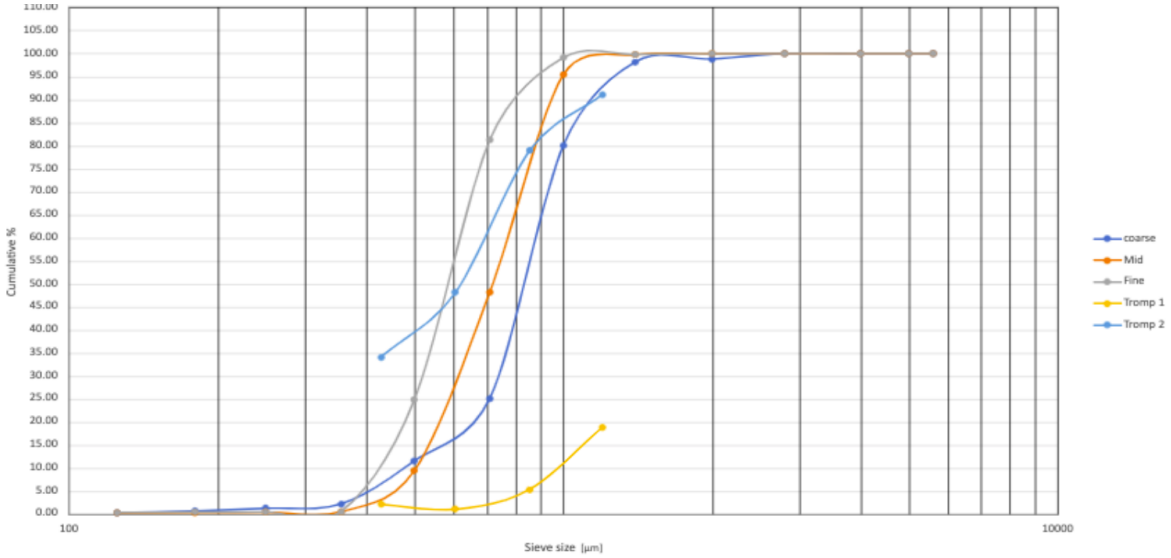

Figure 36 PSD and Tromp Curves 0.5-1mm at 12m/s

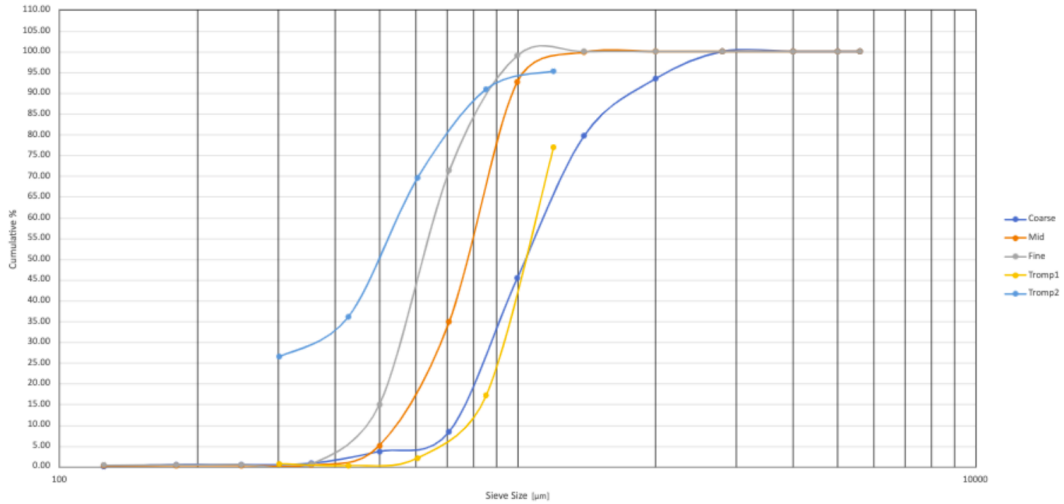

Figure 37 PSD and Tromp Curves 0.5-1mm at 14 m/s

PSD and Tromp curves for SCL 1-3 mm at air velocities 8, 12 and 14 m/s:

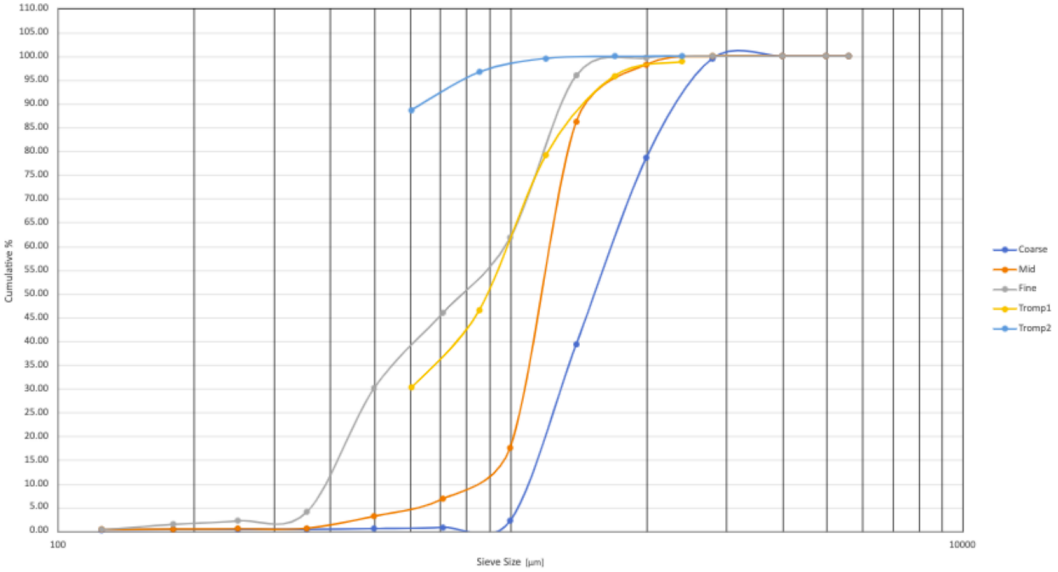

Figure 38 PSD and Tromp Curves 1-3mm at 8 m/s

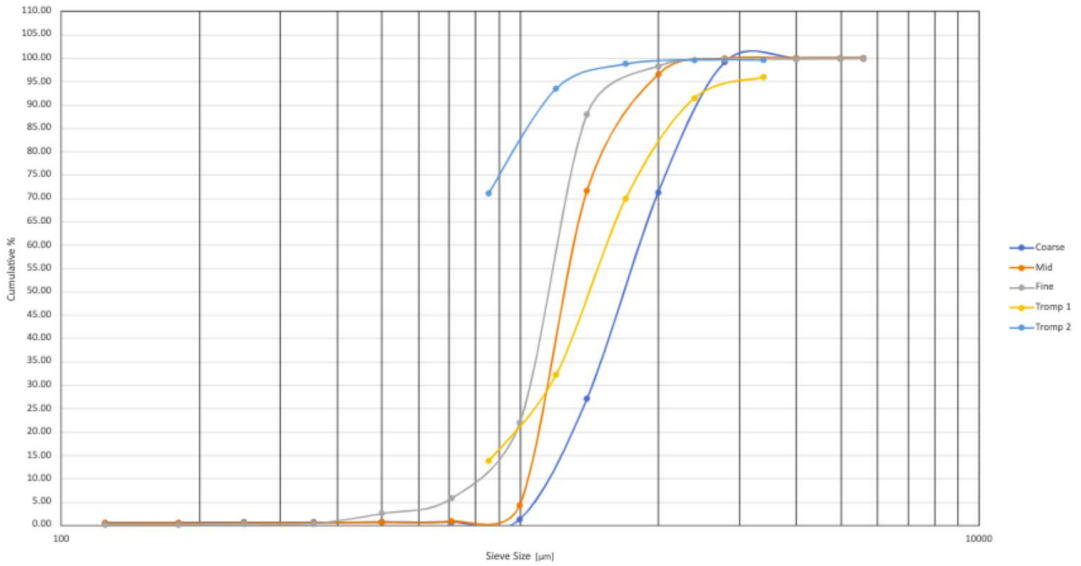

Figure 39 PSD and Tromp Curves 1-3mm at 12m/s

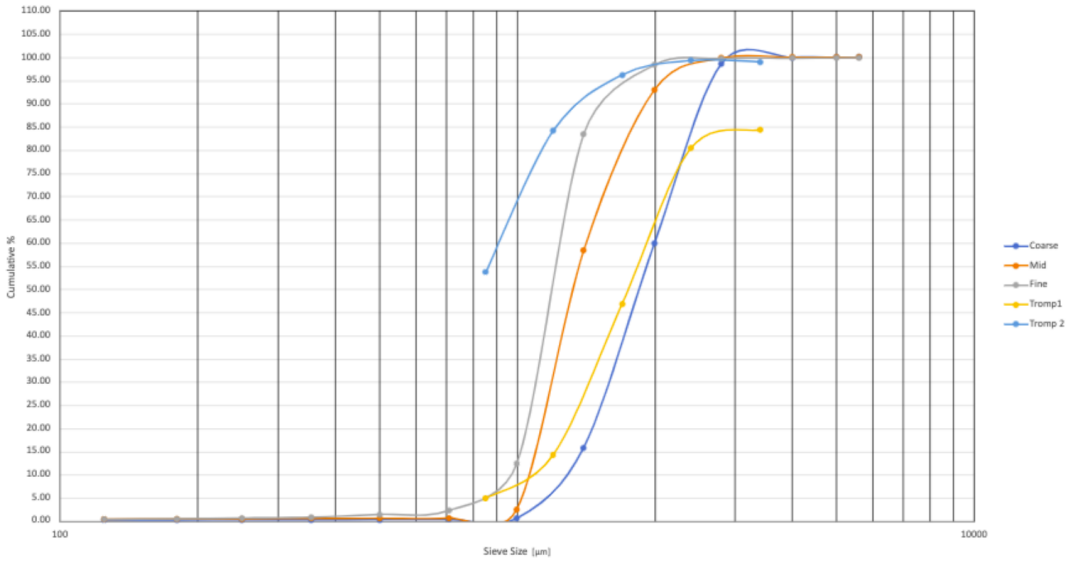

Figure 40 PSD and Tromp Curves 1-3mm at 14m/s

D Alternative Separation Methods

Sieve set

Sieve analysis is a widely used method that is characterized by its ease of use and robust experimental setup. In addition, the reliability of results and good reproducibility are factors that enable consistent analyses. Negative aspects of sieve analysis are the high manual effort and the time required [13].

In sieve analysis, the particle characteristic of geometric size is used. Dry sieving covers a grain size range from 20 µm to 10 mm; finer materials are examined using wet sieving. The method and the size distribution within the sample determine the amount added, which can range from less than 10 g to a few kilograms. The relative movement between the sieve mesh and the feed material determines the actual separation process between coarse and fine material. Particles that are larger than the mesh size cannot pass through the sieve and remain as a residue on the fabric; finer material can pass through the gaps in the fabric and is referred to as a passage. Figure 41 shows the so-called sieve set method, which was used in the processing tests. The fabrics are arranged from coarse to fine and the passage through the upper sieve is the feed quantity for the sieve below [13].

Figure 41 Sieve set at the Chair of Mineral Processing, Montanuniversitaet Leoben.

The grain shape has a decisive influence on the result of a sieve analysis. Many theoretical assumptions assume ideal, spherical particles whose shape factor is f = 1. The form factor is defined as the ratio of the actual surface of a particle to the surface of a sphere of the same volume. Real particles always deviate from an ideal spherical shape and therefore have form factors f > 1. For example, with elongated particles such as rice grains, the greatest longitudinal extent of the grain prevents it from

passing through the sieve mesh along this axis. However, if the rice grain is rotated 90° along the vertical spatial axis, the grain can potentially pass through the same sieve plane. As a result, accumulation processes of characteristically shaped grains can occur in special grain classes [14].

Air separation table (dry process) and lab shaking table (wet process)

The air separation table (also air stove, fluid bed separator or aero stove) is used in waste processing, e.g. for recycling cable scrap (see Figure 42). The most relevant component is the so-called stove plate (also feed surface). This has grooves with holes all over the surface and can be rectangular, trapezoidal or V-shaped. The surface is inclined along the longer side and compressed air flows through the holes. The motorized movement of the plate, in combination with the air flow, leads to density sorting [15].

At the beginning of the process, the feed material lies on the stovetop as a bed. After the material has been fluidized by the compressed air, several forces act on the particles, which sort them depending on the critical influencing variables such as density, mass and grain shape. Here, particles of higher density are transported upwards into the heavy material and particles of lower density are transported downwards into the light material. The inflow area of the particles is another crucial influencing factor for sorting. Flat-shaped particles have a significantly higher flow area in relation to the particle mass than, for example, wires. This larger area leads to a stronger buoyancy force on the particle, causing these particles to lose contact with the stovetop. Particles with a larger inflow area therefore tend to be discharged downwards [16].

Figure 42 Air separation table at the Chair of Mineral Processing, Montanuniversitaet Leoben.

The principle of the lab shaking table is similar, the only difference to the air separation table is that the fluidized bed is water instead of compressed air. The lab shaking table to be used can be seen in Figure 43.

Figure 43 Lab shaking table at the Chair of Mineral Processing, Montanuniversitaet Leoben.

Corona drum separator

The corona drum separator is a unit for electrical sorting; the feed material is separated into conductor, non-conductor and mixed fractions (see Figure 44). This results in a negative charge of all grains, regardless of their electrical conductivity, in the effective area of the corona current [17].

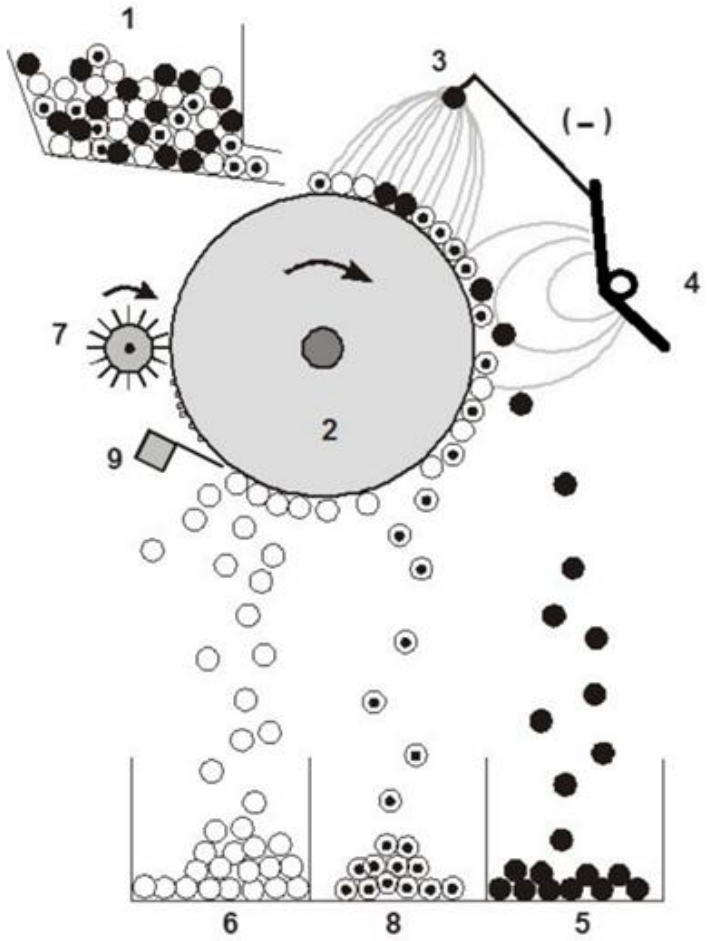

Figure 44 How the corona drum separator works, 1…material feed, 2…drum, 3…corona electrode, 4…field electrode, 5…conductor fraction, 6…non-conductor fraction, 7…brush, 8…mixed fraction, 9…scraper [18]

When the grains leave the area of the corona flow, they initially remain in contact with the rotating roller. However, electrical contact with the roller is only maintained with conductive and semiconducting grains; only they exchange charge with the drum electrode. This allows them to release their charge; the resulting throwing trajectories of the grains can be seen in Figure 44. The non-conductive grains adhere to the roller due to the binding forces that continue to act, which are first released by the scraper and then reach the non-conductor fraction. The conductive particles do not adhere due to their discharge and are transported into the conductor fraction through their trajectory. The mixed fraction is located between the conductor and non-conductor fractions [17].

Flotation

The characteristic of froth flotation, carried out predominantly in mechanical flotation cells, is that a froth is produced which is loaded with solids by bubble-particle contact [17]. Flotation is often applied for complex ores with low grades where liberation is only received by fine grinding. In mechanical flotation cells, where air is introduced through an impeller, the discharge of the froth product is accomplished by direct overflow. It has to be considered that each application is a special case with its unique combination of minerals and water chemistry and therefore requires the selection of individual flotation reagents. Flotation is a process which utilises hydrophobic surfaces to provide bubble-particle attachment, therefore surface wettability is the limiting factor. A few minerals, like graphite, are naturally hydrophobic. Collectors are organic molecules that selectively absorb on mineral surfaces and act hydrophilizing. A frother is necessary to generate a stable froth and to avoid inadequate froth breakage. Frothers are organic reagents with a polar group for water solubility and a nonpolar

hydrocarbon group. On the one hand particles can enter the froth by attachment to bubbles, on the other hand by entrainment in the water due to rising bubbles. This means that unwanted particles (gangue), especially of finer particle sizes, are trapped in the froth and join the product. Therefore, a large amount of fines and slime fraction impacts the flotation of coarser particles. In many cases water sprays are installed above the froth. Depressants are hydrophilic molecules that avoid adsorption of particles on bubbles. The equipment to be used for the trials can be seen in Figure 45.

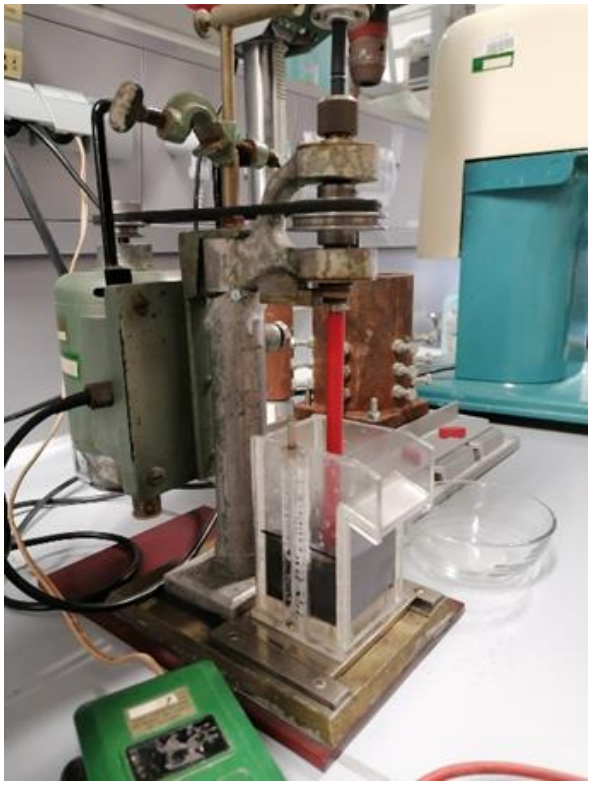

Figure 45 Flotation equipment at the Chair of Mineral Processing, Montanuniversitaet Leoben.